

1 **Title**

2 Aerobic exercise reverses aging-induced depth-dependent decline in cerebral microcirculation

3 **Authors**

4 Paul Shin^{1*}, Qi Pian¹, Hidehiro Ishikawa², Gen Hamanaka², Emiri T Mandeville², Guo Shuzhen², Fu Buyin¹,
5 Mohammed Alfadhel^{1,3}, Srinivasa Rao Allu^{4,5}, Ikbal Şencan-Eğilmez^{1,6}, Baoqiang Li^{7,1}, Chongzhao Ran¹, Sergei
6 A Vinogradov^{4,5}, Cenk Ayata^{8,9}, Eng H Lo², Ken Arai², Anna Devor^{10,1}, and Sava Sakadžić¹

7 ¹*Athinoula A. Martinos Center for Biomedical Imaging, Massachusetts General Hospital, Harvard Medical School, Charlestown, MA, USA*

8 ²*Neuroprotection Research Laboratory, Departments of Radiology and Neurology, Massachusetts General Hospital, Harvard Medical
9 School, Charlestown, MA, USA*

10 ³*Department of Bioengineering, Northeastern University, Boston, MA, USA*

11 ⁴*Department of Biochemistry and Biophysics, University of Pennsylvania, Philadelphia, PA, USA*

12 ⁵*Department of Chemistry, University of Pennsylvania, Philadelphia, PA, USA*

13 ⁶*Biophotonics Research Center, Mallinckrodt Institute of Radiology, Department of Radiology, Washington University School of Medicine,
14 St. Louis, MO, USA*

15 ⁷*Brain Cognition and Brain Disease Institute, Shenzhen Institute of Advanced Technology, Chinese Academy of Sciences, Shenzhen,
16 Guangdong, China*

17 ⁸*Neurovascular Research Laboratory, Department of Radiology, Massachusetts General Hospital, Harvard Medical School, Charlestown,
18 MA, USA*

19 ⁹*Stroke Service, Department of Neurology, Massachusetts General Hospital, Harvard Medical School, Charlestown, MA, USA*

20 ¹⁰*Department of Biomedical Engineering, Boston University, Boston, MA, USA*

21 *Corresponding author: pshin2@mgh.harvard.edu

22

23

24 ***Abstract***

25 Aging is a major risk factor for cognitive impairment. Aerobic exercise benefits brain function and may promote
26 cognitive health in older adults. However, underlying biological mechanisms across cerebral gray and white matter
27 are poorly understood. Selective vulnerability of the white matter to small vessel disease and a link between white
28 matter health and cognitive function suggests a potential role for responses in deep cerebral microcirculation.
29 Here, we tested whether aerobic exercise modulates cerebral microcirculatory changes induced by aging. To this
30 end, we carried out a comprehensive quantitative examination of changes in cerebral microvascular physiology
31 in cortical gray and subcortical white matter in mice (3-6 vs. 19-21 months old), and asked whether and how
32 exercise may rescue age-induced deficits. In the sedentary group, aging caused a more severe decline in cerebral
33 microvascular perfusion and oxygenation in deep (infragranular) cortical layers and subcortical white matter
34 compared with superficial (supragranular) cortical layers. Five months of voluntary aerobic exercise partly
35 renormalized microvascular perfusion and oxygenation in aged mice in a depth-dependent manner, and brought
36 these spatial distributions closer to those of young adult sedentary mice. These microcirculatory effects were
37 accompanied by an improvement in cognitive function. Our work demonstrates the selective vulnerability of the
38 deep cortex and subcortical white matter to aging-induced decline in microcirculation, as well as the
39 responsiveness of these regions to aerobic exercise.

40

41 ***1. Introduction***

42 The cerebral white matter is significantly affected by-aging.(Cees De Groot et al., 2000; de Leeuw et al., 2001)
43 Previous work suggests that, in comparison with superficial gray matter, subcortical white matter has greater tissue
44 loss due to aging and is more susceptible to hypoperfusion.(Gunning-Dixon et al., 2009; Hase et al., 2019; Li et
45 al., 2020) Indeed, white matter lesions might impair cognitive function more than gray matter lesions,(Reber et
46 al., 2021) underscoring the importance of understanding the biological mechanisms of aging related white matter
47 degeneration for targeted interventions.

48 Cerebral small vessel disease (CSVD) refers to a range of pathological processes affecting small
49 arterioles, capillaries, and venules supplying the white matter and deep structures of the brain. CSVD is a common
50 cause of stroke and an important contributor to age-related cognitive decline and dementia.(Pantoni, 2010; Smith
51 & Markus, 2020) Most CSVD related strokes affect subcortical white and deep gray matter. In addition, there is
52 increased awareness of the role of CSVD in accelerating the pathogenesis of Alzheimer’s disease (AD), with some
53 studies suggesting the possibility that white matter changes are the starting point of AD.(Defrancesco et al., 2014;
54 Esiri et al., 1999; Radanovic et al., 2013; Snowden et al., 2011) Despite this growing awareness, our mechanistic
55 understanding of aging-related changes in microcirculation as a function of depth in cortex and underlying white
56 matter is incomplete.

57 Aerobic exercise is a promising strategy to improve neurocognitive function in aging and reduce the
58 risk of age-related neurological disorders.(D. E. Barnes et al., 2003; Yaffe et al., 2001) Most studies have thus far
59 focused on exercise-responsive molecules that could lead to improvement of neural physiology and, thereby,
60 cognitive performance.(de Miguel et al., 2021; Islam et al., 2021; Valenzuela et al., 2020; Wang & Holsinger,
61 2018) Yet, how exercise may exert beneficial effects on vascular contributions to brain aging remain to be fully
62 understood. In particular, it is unclear how exercise normalizes cerebral microcirculation, and whether there are
63 differential effect across brain regions, including the gray and white matter.

64 In this study, we compared young (3-6 month old) vs. old (19-21 months old) mice to assess the effects
65 of normal aging, and then asked whether 5 months of voluntary aerobic exercise can alter or rescue brain
66 microcirculation in old 20-month-old mice. Cerebral microvascular perfusion and oxygenation in the cortex and
67 subcortical white matter was quantified with two-photon microscopy (2PM) and optical coherence tomography
68 (OCT) in awake mice.

69 Our results showed age-related declines in capillary red-blood-cell (RBC) flux and capillary oxygen
70 partial pressure (pO_2) in the deep cortical layers and subcortical white matter, while voluntary exercise improved
71 these measures, including the cerebral blood flow (CBF) in cortical ascending venules. Interestingly, the regions
72 that experienced the highest decline were also the ones that benefited the most from the exercise. These
73 microcirculatory effects were accompanied by an improvement in cognitive function. Our results may provide
74 insights into how sedentary aging and aerobic exercise affect cerebral microvascular physiology and particularly
75 emphasize the physiologic importance of effects in the deep cortex and subcortical white matter.

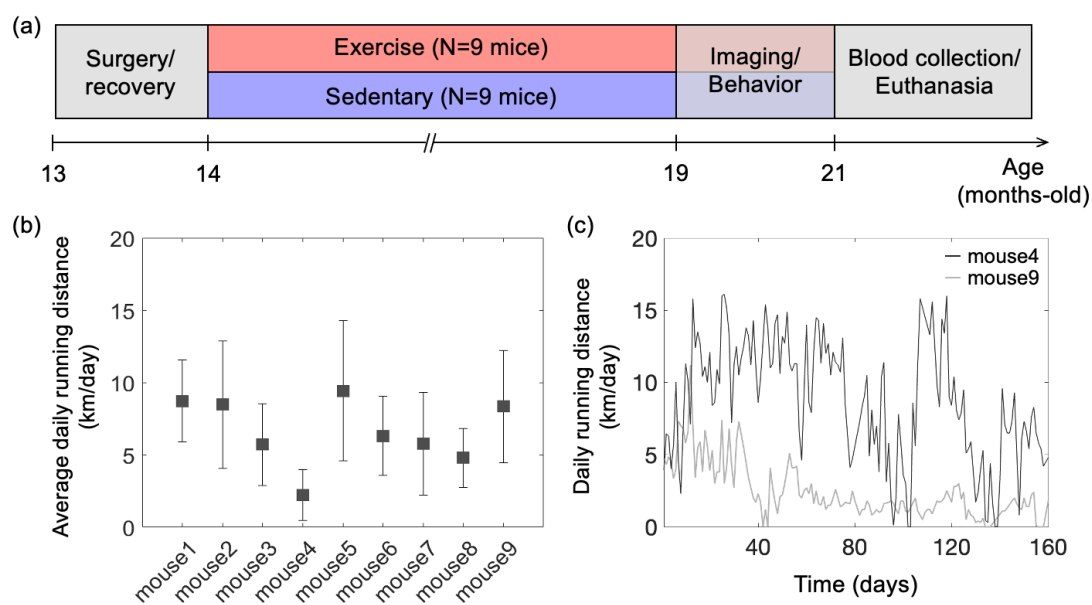
76

77 **2. Methods**

78 *2.1 Animal preparation and experimental protocol*

79 All animal surgical and experimental procedures were conducted following the Guide for the Care and
80 Use of Laboratory Animals and approved by the Massachusetts General Hospital Subcommittee on Research
81 Animal Care. All efforts were made to minimize the number of animals used and their suffering, in accordance
82 with the Animal Research: Reporting in Vivo Experiments (ARRIVE) guidelines. Female C57BL/6N mice (n=18,
83 12 months old) were obtained from National Institute on Aging colonies. The experimental timeline of the study
84 is shown in Figure 1a. A chronic cranial window (round shape, 3 mm in diameter) was implanted on the left
85 hemisphere, centered over the E1 whisker barrel (2.0 mm posterior to bregma and 3.0 mm lateral from the midline)
86 at the age of 13 months. Mice were allowed four weeks to recover fully from surgery. Next, mice were randomly
87 divided into two groups (exercise: n=9; sedentary: n=9), and all mice were housed individually. Cages of mice in
88 the exercise group were equipped with wireless running wheels (ENV-047; Med Associates) that could be used
89 by mice at any time. The total number of wheel rotations was recorded daily through a wireless hub device (DIG-
90 807; Med Associates). For each mouse in the exercise group, the wheel running activity was characterized based
91 on the intensity of exercise, defined as the average daily running distance over five months (Figures 1b,c). After
92 five months of voluntary exercise (or standard housing for the sedentary controls), mice underwent restraint
93 training for awake imaging. Mice in the exercise group were continuously housed in cages with running wheels
94 during both training and imaging weeks. All mice were gradually habituated to longer restraint periods, up to 2
95 hours. They were rewarded with sweetened milk every ~15 min during training and imaging. Optical
96 measurements were performed between 19 and 21 months of age. The measurements were performed during 5-6
97 weeks in the following order: two-photon phosphorescence pO₂ imaging, 2PM angiography, optical intrinsic
98 signal imaging (OISI), 2PM imaging of capillary RBC flux, and Doppler OCT. 7-10 days of a break was given
99 between measurements in each animal. Finally, behavioral tests were performed, and blood samples were collected
100 from the animals for hematocrit (Hct) measurements before the animals were euthanized.

101 Some measurements in the old mice were compared with similar measurements in the young adult mice.
102 Female C57BL/6N mice, 6-month-old (n=8) for OISI (OISI group) and 3-month-old (n=3) for capillary RBC flux
103 imaging (2PM group), were used in this work. Chronic cranial window implantation, animal recovery from the
104 surgery, and restraint training were performed following the same protocols as in the old mice. Therefore,
105 measurements were performed at 7 months in the OISI group and 4 months in the 2PM group.

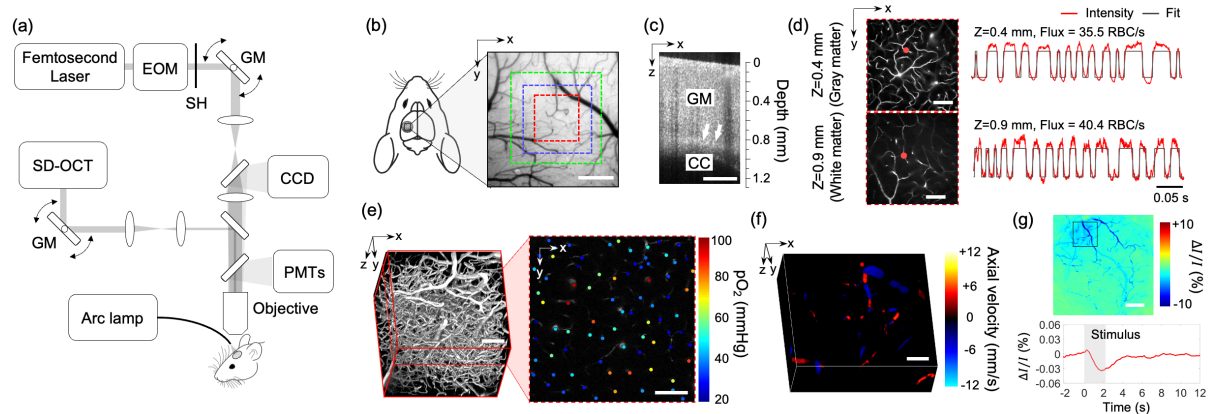


106

107 [Figure 1] Animal preparation and experiment design. (a) Timeline of the study. Optical measurements and
108 behavioral testing were performed after 5 months of voluntary exercise when the animals were 19-21 months of
109 age. (b) Average daily running distance in km per day for each mouse in the exercise group, calculated as the sum
110 of daily running distance divided by a total running period of 5 months. Data are shown as mean \pm SD. (c) Daily
111 running distance for two representative mice in the exercise group across time.

112 2.2 Multimodal optical imaging in awake mice at rest

113 In this study, we employed our previously described home-built multimodal imaging system that features multiple
114 optical imaging capabilities, including 2PM, OCT, and OISI.³ Figure 2a shows a schematic of the multimodal
115 imaging system. All optical measurements were made in the head-restrained awake mice at rest. The
116 measurements were conducted while mice were resting on a suspended soft fabric bed in a home-built imaging
117 platform. An accelerometer was attached to the suspended bed to monitor the signals induced by animal motion.
118 Data affected by the motion were rejected during data processing based on the signal generated by the
119 accelerometer. The data acquired when the accelerometer reading exceeded the threshold value, which was
120 determined empirically by comparing signals obtained during stationary and movement periods, were rejected
121 from the analysis. During the experiments, animal behavior was continuously monitored using a web camera
122 (LifeCam Cinema; Microsoft) with a LED illumination at 940 nm, and a reward (sweetened milk) was offered
123 every ~15 min. Experiments were terminated if signs of discomfort or anxiety were observed.



124

125 [Figure 2] Experimental setup and imaging protocols. (a) Schematic of our home-built multimodal optical system
 126 featuring primary components of the system. A 50 kHz spectral-domain OCT system was designed to partially
 127 share the imaging optics with the two-photon microscope. A Hg:Xe arc lamp in combination with a CCD camera
 128 was used for OISI. EOM: electro-optic modulator, SH: shutter, GM: galvanometer mirror pair. (b) A CCD image
 129 of brain surface vasculature in the mouse barrel cortex showing the ROIs where various optical measurements
 130 were performed (red ROI: capillary RBC flux, pO₂, and microvasculature imaging, blue ROI: Doppler OCT
 131 imaging, and green ROI: OCT intensity imaging). (c) A representative OCT intensity B-scan image extracted from
 132 a volumetric OCT image. White arrows indicate the boundary between the gray matter (GM) and the corpus
 133 callosum (CC), which appears as a bright band in the image. (d) Survey scan images of cerebral microvasculature
 134 of the region outlined with the red square in (b) obtained by two-photon microscope at two imaging depths (z=0.4
 135 and 0.9 mm). Two representative fluorescent intensity time courses acquired within the capillaries at the locations
 136 indicated by the red dots in the survey angiograms are presented on the right. (e) A 3D angiogram of the mouse
 137 cortex acquired by the two-photon microscope at the location outlined by the red square in (b). One representative
 138 2D plane from the angiogram acquired at a depth of 200 μm showing pO₂ measurements from different capillary
 139 segments. pO₂ values were color-coded (in mmHg) and spatially co-registered with the angiogram. (f) A 3D
 140 Doppler OCT image showing an axial velocity map of the diving vessels at the location outlined by the blue square
 141 in (b). (g) An OIS image of the cranial window obtained by calculating the relative intensity difference between
 142 the post-stimulus response image and pre-stimulus baseline. The region of activation is manually selected from
 143 the OIS image as indicated by a black square. The lower panel shows a time course of the relative intensity change
 144 due to sensory-evoked hemodynamic response induced by a 2-s-long whisker stimulation, averaged over the
 145 selected region of interest. Scale bars: 400 μm for (b) and (c), 100 μm for (d), (e), and (f), and 500 μm for (g).

146 *2.3 Two-photon microscope for fluorescence and phosphorescence imaging*

147 A two-photon microscope integrated into our multimodal imaging system was used for capillary RBC flux
148 measurements and 3D microvascular angiography(Li et al., n.d.; Sakadžić et al., 2010). A pulsed laser (InSight
149 DeepSee; Spectra-Physics, tuning range: 680 nm to 1300 nm, ~120 fs pulse width, 80 MHz pulse repetition rate)
150 was used as an excitation light source. Laser power was controlled by an electro-optic modulator (EOM) (350-
151 160; ConOptics, Inc.). The laser beam was focused by a water immersion objective lens (XLUMPLFLN20XW;
152 Olympus) and scanned in the transverse (X-Y) plane by a pair of galvanometer mirrors (Saturn 5B; Pangolin Laser
153 System, Inc.). The objective lens was translated along the Z-axis by a motorized stage (M-112.1EG; Physik
154 Instrumente) to probe different depths ranging from the brain surface to depths beyond 1 mm below the surface.
155 Emitted fluorescence was directed to detectors by an epi-dichroic mirror (FF875-Di01-38.1×51; Semrock Inc.)
156 positioned above the objective, followed by an infrared blocker (FF01-890/SP-50; Semrock Inc.). The four-
157 channel detector consists of four photomultiplier tubes (PMTs) paired with emission filters that cover a wide range
158 of emission wavelengths. One detector channel with a PMT exhibiting a red-shifted spectral response
159 (H10770PA-50; Hamamatsu) and a 709/167 nm emission filter was connected to a discriminator (C9744;
160 Hamamatsu) and used for capillary RBC flux measurements. Another channel with a multialkali photocathode
161 PMT (R3896; Hamamatsu) and a 525/50 nm emission filter was used for two-photon angiography.

162 We employed another home-built two-photon microscope for intravascular pO₂ measurements. The
163 second 2PM employs a Ti:Sapphire mode-locked laser (Mai Tai HP; Spectral Physics, tuning range: 690 nm to
164 1040 nm, ~100 fs pulse width, 80 MHz pulse repetition rate) as a light source. The output laser power delivered
165 to the sample is modulated with EOM (350-105-02; ConOptics Inc.). The transverse scanning was achieved by a
166 two-axis 7-mm galvanometer scanner (6210H; Cambridge Technology). The laser beam was relayed to the back
167 focal plane of the objective through the combination of a scan lens (f = 51 mm, 2x AC508-100-B, Thorlabs) and
168 a tube lens (f=180 mm, Olympus). The Z-axis movement of the objective was controlled by two translation stages
169 (ZFM2020 and PFM450E; Thorlabs). The phosphorescence emission signal from the sample was filtered by a
170 dichroic mirror (FF875-Di01-38.1X51; Semrock Inc.) and an emission filter (FF01-795/150-25; Semrock Inc.)
171 before detected by a PMT (H10770PA-50; Hamamatsu) and a photon counting unit (C9744; Hamamatsu).

172 The objective lens was heated by an electric heater (TC-HLS-05; Bioscience Tools) throughout the
173 measurement to maintain the temperature of the water between the objective lens and the cranial window at 36-
174 37 °C.

175 *2.4 Spectral-domain OCT*

176 A low-coherence superluminescent diode with a center wavelength of 1300 nm was used as the light source
177 (S5FC-1018S; Thorlabs). The line scan camera was operated with a 50 kHz acquisition rate (GL2048L; Sensors
178 Unlimited). The sample arm of the system partially shares the imaging optics with the two-photon microscope,
179 but it utilizes separate scanning optics, as shown in Figure 2a. The system has an axial resolution of 10 μm in
180 tissue. The transverse resolution is 7 μm using a 10 \times objective lens (Mitutoyo Plan Apo NIR; Edmund Optics).
181 The incident optical power on the sample was 5 mW. For OCT Doppler measurements, the maximum measurable
182 flow speed without phase wrapping was ± 12 mm/s when the direction of flow was parallel to the OCT beam and
183 the minimum detectable velocity was ± 0.7 mm/s which was determined by the phase noise of the system,
184 measured as ± 0.2 radians.

185 *2.5 OISI system*

186 A Hg:Xe arc lamp (66883; Newport) was used in combination with a band-pass filter (570/10 nm) for OISI. A
187 4 \times objective lens (XLFLUOR4X/340; Olympus) was used to achieve a wide field-of-view (FOV) that covered
188 the entire cranial window. Two-dimensional images of the cranial window were acquired using a CCD camera
189 with 100 ms exposure time (acA1300; Basler).

190 *2.6 Measurements of capillary RBC flux, speed, and line-density in gray and white matter*

191 Before imaging, the dextran-conjugated Alexa680 solution (70 kDa, 0.1-0.15 ml at 5% W/V in PBS; Thermo
192 Fisher Scientific) was retro-orbitally injected into the bloodstream. Figure 2b shows a CCD image of the mouse
193 cranial window positioned on the left somatosensory cortex. A volumetric OCT scan was performed with a FOV
194 of 1×1 mm² over the region shown with a green square box in Figure 2b. The acquired OCT volume was used to
195 identify the boundary between the gray and white matter and measure the cortical thickness as we previously
196 described (Figure 2c). (Li et al., 2020) After confirming localization of the white matter, 2PM was performed over
197 the same region as for the OCT imaging, but with a smaller FOV of 500×500 μm^2 indicated by a red square
198 region (Figure 2b). The RBC flux measurements in the gray matter were performed at cortical depths of 150 and
199 400 μm , which correspond to layers II/III and IV. In the white matter, measurements were performed at a depth
200 of 0.9-1.1 mm. Awake imaging lasted less than 2 hours and the flux measurements were performed only at three
201 depths due to the time spent performing the OCT imaging prior to the flux measurements. At each depth, a survey
202 image of the vasculature was acquired by raster scanning the beam across the FOV (Figure 2d). Then we manually
203 selected measurement locations inside all the capillary segments identified within the survey image. Capillaries

204 were identified based on their network structure and, in this work, all branching vessels from diving arterioles and
205 surfacing venules were defined as capillaries. The laser beam was parked at each location for 0.9 s and the
206 fluorescence signal was detected in the photon-counting mode. The photon counts were binned into 300- μ s-wide
207 bins, resulting in a fluorescence intensity time course with 3,000 time points. Figure 2d shows representative
208 fluorescence signal transients taken from two measurement locations at different depths. Following the procedures
209 described in our previous study,(Li et al., 2020) the fluorescence signal time course was segmented with a binary
210 thresholding approach (red curve in Figure 2d) and RBC flux was calculated by counting the number of valleys
211 in the segmented curve normalized by the acquisition time. Following our previously described procedures,(Li et
212 al., n.d.) RBC speed for each RBC-passage event (valley) in the segmented curve was estimated as $v = D/\Delta t$,
213 where D is RBC diameter, assumed to be 6 μ m, and Δt is the width of the valley. For each capillary, the speed
214 values estimated from each of the valleys in the segmented curve were averaged to obtain the mean RBC speed.
215 Finally, RBC line-density was calculated as the ratio between combined time duration of all valleys to the total
216 duration of the entire time course.

217 *2.7 Intravascular pO₂ imaging and calculation of SO₂ and depth-dependent OEF*

218 A phosphorescent oxygen-sensitive probe Oxyphor2P was diluted in saline and retro-orbitally injected before
219 imaging (0.05 ml at ~80 μ M).(Esipova et al., 2019) The pO₂ imaging was performed using 950 nm excitation
220 wavelength and with a FOV of 500 \times 500 μ m² at the same cortical region where the RBC flux measurements
221 were performed (Figure 2b). The measurements were performed at cortical depths from the surface to 450 μ m
222 depth with 50 μ m interval between depth locations. At each depth, two-dimensional raster scan of
223 phosphorescence intensity was performed to acquire a survey image. Then, we manually selected the measurement
224 locations inside all diving arterioles, surfacing venules, and capillary segments visually identified within the
225 survey image. Next, the focus of excitation laser beam was parked at each selected segment to excite the
226 Oxyphor2P with a 10- μ s-long excitation gate. The resulting emitted phosphorescence was acquired during 290-
227 μ s-long collection time. Such 300- μ s-long cycle was repeated 2,000 times to generate an average phosphorescence
228 decay curve. The averaged curve was fitted to a single-exponential decay, and the lifetime was converted into
229 absolute pO₂ using a Stern-Volmer-like expression obtained from independent calibrations.(Esipova et al., 2019;
230 Li et al., n.d., 2020; Şencan et al., 2022) The oxygen saturation of hemoglobin (SO₂) and the depth-dependent
231 oxygen extraction fraction (DOEF) were computed following our previously described procedures.(Li et al., n.d.)
232 Briefly, the SO₂ was calculated using the Hill equation based on the measured pO₂ and the DOEF was calculated

233 as $(SO_{2,A} - SO_{2,V})/SO_{2,A}$, where $SO_{2,A}$ and $SO_{2,V}$ represent the mean SO_2 in the diving arterioles and surfacing
234 venules in a given cortical layer, respectively.

235 *2.8 Characterization of morphological changes in cortical capillaries*

236 FITC-dextran (Thermo Fisher Scientific, 70 kDa) was diluted in saline and injected retro-orbitally before imaging
237 (, 0.05 ml at 5% W/V). A three-dimensional imaging of the cortical vasculature was performed with 500×500
238 μm^2 FOV to cover the same region of interest (ROI) used for capillary flux and pO_2 measurements (Figure 2e).
239 The microvascular stack was generated by repeatedly acquiring images with the axial steps of 1 μm up to a depth
240 of 400 μm . In each animal, a smaller ROI ($200 \times 200 \mu\text{m}^2$) was manually selected to cover the region containing
241 mostly capillaries (e.g., capillary bed area). A 3D microvasculature corresponding to the selected ROI was
242 segmented using a vessel segmentation algorithm, VIDA,(Tsai et al., 2009) and the number of capillary segments
243 per volume (e.g., vessel segment density) and the average capillary segment length per volume (e.g., vessel
244 segment length density) were calculated. The vessel segment was defined as the part of the vessel between two
245 consecutive branching points.

246 *2.9 Quantitative flow measurements using Doppler OCT*

247 A total of 20 Doppler OCT volumes were continuously acquired with a $750 \times 750 \mu\text{m}^2$ FOV at the region
248 indicated by a blue square box in Figure 2b. 10 volumes exhibiting minimal motion artefacts were selected and
249 averaged to generate a single Doppler OCT volume. Each Doppler OCT volume was comprised of 300 B-scans,
250 where 3,000 A-scans were acquired per B-scan. The Doppler volume yields a three-dimensional map of the z-
251 projection of RBC velocity (Figure 2f). For each depth slice in the volume, we measured flow in each surfacing
252 venule over the FOV by estimating the integral of the velocity projection over the vessel cross section following
253 the protocol previously described.(Srinivasan et al., 2011) We used 3D angiograms acquired by 2PM (see Method
254 2.7 for more details) to estimate the diameter of the vessels, used for cross-correlation analysis between the flow
255 and vessel diameter. The measured flow values in each vascular segment were averaged within the depth range
256 of 50-100 μm . Flow data measured in diving arterioles were excluded from analysis due to their much higher flow
257 compared to venular flow that often causes excessive phase wrapping and signal fading.(Koch et al., 2009)

258 *2.10 OISI imaging of hemodynamic response to functional activation*

259 Two-dimensional CCD images were continuously acquired with a CCD camera for 18 seconds. Five seconds after

260 the onset of image acquisition, a whisker stimulus was applied at 3 Hz for 2 s. A total of 20 stimulation trials were
261 repeated with an inter-stimulus interval of 25 seconds. Among 20 trials, the data acquired during excessive animal
262 motion (~10% of the measurements) were excluded from analysis based on a threshold criterion applied to the
263 accelerometer recordings. Bulk motion artifacts in the acquired CCD images caused by small transverse
264 movement ($< \sim 50 \mu\text{m}$) were compensated by 2D cross-correlation based motion correction algorithm.(Guizar-
265 Sicairos et al., 2008) After motion compensation, images were averaged over trials before computing the fractional
266 intensity difference between the response and baseline images (Figure 2g) as described in our previous
267 work.(Şencan et al., 2022)

268 *2.11 Behavioral tests*

269 A novel object recognition test (NORT) was performed to evaluate whether exercise improves short-term memory
270 in old mice. Briefly, mice were allowed to explore two identical objects in a testing arena for 5 minutes and
271 returned to their home cage for 30 minutes. Mice were then moved back to the arena with one of the objects
272 replaced with a novel object and allowed to explore the objects for 5 minutes. Behavioral performance was
273 evaluated by estimating the discrimination index (DI). The DI was defined as exploration time of the novel object
274 normalized by combined exploration time of both objects and was calculated during four different time intervals
275 in each animal: during first one, two, three, and five minutes of the object exploration.

276 Y-maze test was used to measure the willingness of animals to explore new environments and spatial
277 working memory. The testing occurred in a Y-shaped maze with three arms at a 120° angle from each other. Mice
278 were placed at the center of the maze and allowed to freely explore the three arms for 10 minutes. The number of
279 arm entries and the number of triads (consecutive entries into three different arms) were measured to calculate the
280 percentage of spontaneous alteration, defined as the ratio of the number of alternating triads to total number of
281 arm entries -2.

282 *2.12 Hct measurements*

283 Hct measurements were carried out by a blood gas analyzer (OPTI CCA-TS2; OPTI Medical Systems) using a B-
284 type cassette. Mice were anesthetized with 2% isoflurane, and then approximately 250 μl of venous blood was
285 collected from the inferior vena cava. The collected blood was aliquoted into two 100 μl capillary tubes. The Hct
286 measurement was performed two times with each blood sample and the average of the two measurements was
287 reported.

288 *2.13 Statistical analysis*

289 Statistical analysis was carried out using t-test or ANOVA (MATLAB, MathWorks Inc.). P value less than 0.05
290 was considered statistically significant. Details about the statistical analysis are provided in the figure legends and
291 text, where relevant. Boxplots show the median value with a black line and the mean value with a plus symbol
292 (+). Each box spans between the 25th and the 75th percentile of the data, defined as interquartile range (IQR).
293 Whiskers of the boxplots extend from the lowest datum within 1.5 times the IQR of the lower quartile of the data
294 to the highest datum within 1.5 times the IQR of the highest quartile of the data. For each parameter measured in
295 this study, the acquired values were averaged to obtain the mean value for each mouse, and then the mean values
296 were averaged over mice. Sample size (i.e., n=9 mice for aged sedentary and exercise group) were selected based
297 on the assumption that the most demanding one is to detect 30% difference between the mean capillary pO₂ values
298 (coefficient of variance=0.3, power=0.8, significance=0.05).

299

300 **3. Results**

301 *3.1 Exercise mitigates age-related decline of capillary RBC flux and induces capillary flow homogenization in*
302 *the subcortical white matter*

303 To examine the impact of aging on cortical and subcortical microcirculation, we examined the spatial distribution
304 of capillary RBC flux across cortical and subcortical regions in aged mice and compared the result with
305 measurements from awake C57BL/6N female mice of younger age (4 months old).

306 Capillary RBC flux measurements were conducted using 2PM imaging of RBC-induced shadows within
307 blood plasma labeled by the Alexa-680, allowing the deep imaging into the subcortical white matter down to a
308 depth of ~1.1 mm.(Li et al., n.d.) The mean capillary RBC flux in aged sedentary mice was significantly lower
309 than that in young sedentary mice in both gray and white matter (Figure 3a,b). Importantly, while in young
310 sedentary mice, the mean white matter RBC flux tended to be slightly higher than the gray matter RBC flux, the
311 relationship appeared reversed in aged sedentary mice, where mean RBC flux in the white matter strongly tended
312 to be lower than RBC flux in the gray matter. This suggests that the microcirculation in the white matter is affected
313 more than microcirculation in the gray matter by age-related changes.

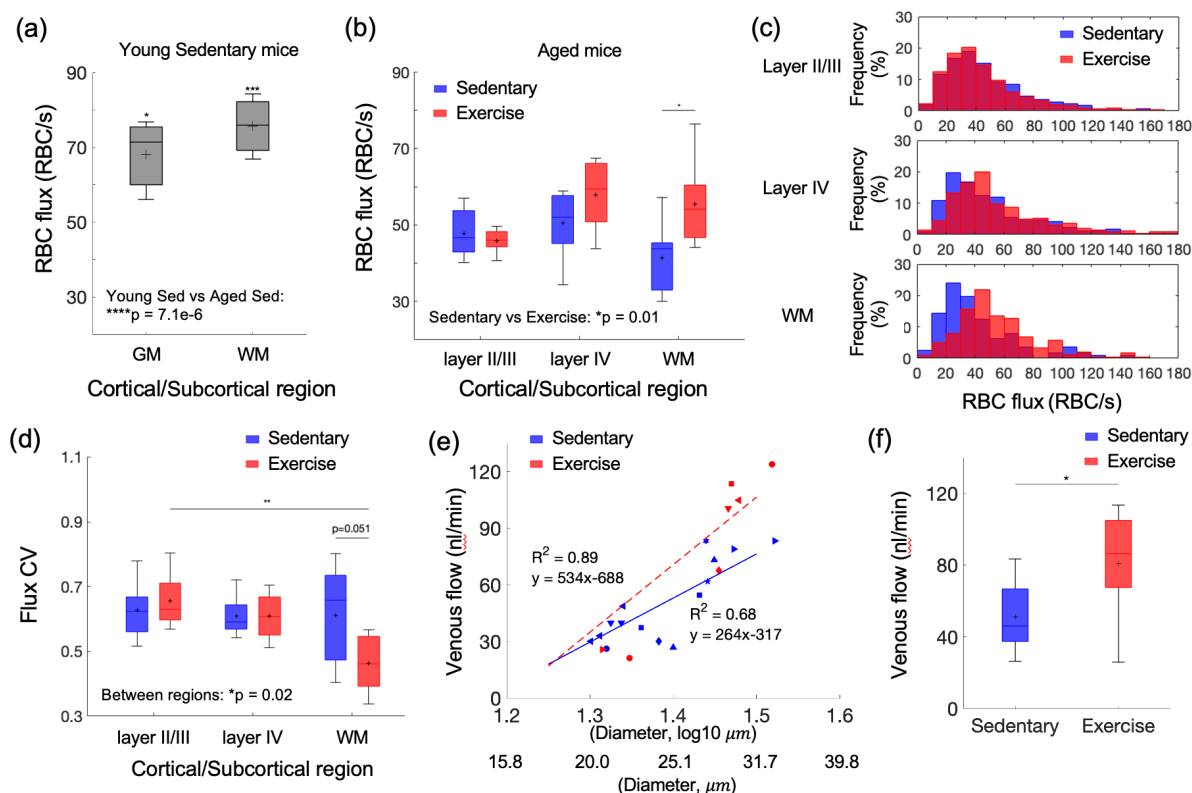
314 We next investigated whether voluntary exercise in aged mice exerts beneficial effects on capillary RBC
315 flux across cortical layers and white matter. We found higher capillary flux in the exercise group compared with
316 sedentary controls, which was most prominent in white matter (Figure 3b) and to a lesser extent in layer IV, while
317 no change was observed in cortical layers II/III. Histograms of capillary RBC flux in gray and whiter matter
318 confirmed this finding (Figure 3c). Exercise also tended to increase capillary RBC speed in layer IV of the cortex
319 and the underlying white matter, while no change was detected in layers II/III (Figure 3 – Figure supplement 1).
320 No significant difference in the RBC line-density between sedentary and exercise group was found (Figure 3 –
321 Figure supplement 2). The RBC line-density of subcortical white matter was significantly higher than the RBC
322 line-density of gray matter in both sedentary and exercise group, consistent with the previous numerical simulation
323 result.(Gould et al., 2017)

324 Exercise decreased the coefficient of variation (CV) of capillary RBC flux in subcortical white matter but
325 not the gray matter, suggesting more homogeneous microvascular blood flow in white matter in the exercise group
326 (Figure 3d). In contrast, we did not find a difference in the CV of capillary RBC flux among the layers in the
327 sedentary group.

328 Finally, we employed Doppler OCT to test the effect of exercise on the blood flow in larger vessels,
 329 particularly the ascending venules in the cortex. We performed a linear regression analysis between the venular
 330 blood flow and the logarithmic vessel diameter (Figure 3e). As expected, a strong correlation was found between
 331 the venular flow and the vessel diameter in both groups, consistent with the previous observation of positive
 332 correlation between venular flow speed and the vessel diameter in mice. (Santisakultarm et al., 2012) Importantly,
 333 the regression slope for the exercise group was steeper than that for the sedentary group ($p=0.005$, analysis of
 334 covariance, ANCOVA). Blood flow in ascending venules was significantly larger (by $\sim 46\%$) in the exercise
 335 group compared to sedentary controls. This result agreed with the improved capillary RBC flux in the white matter
 336 with exercise.

337 The capillary RBC flux in subcortical white matter was moderately negatively correlated with the average
 338 daily running distance (i.e., exercise intensity; $R^2 = 0.31$). No strong correlation was found between other
 339 measured parameters and the exercise intensity (Figure 3 – Figure supplement 3).

340



341

342 [Figure 3] Aging and exercise induced alterations in cerebral microcirculation. (a) Mean capillary RBC flux in
 343 young-adult sedentary mice. The data are from 226 and 218 capillaries in three young sedentary mice in the gray

344 matter (GM) and white matter (WM), respectively. Comparison was made between young and aged sedentary
345 group (shown in (b)) in each gray (layers II/III, IV in aged sedentary group) and white matter region. (b) Capillary
346 RBC flux across cortical layers II/III and IV, and subcortical white matter in aged sedentary and exercise group.
347 (c) Histograms of capillary RBC flux in the gray and white matter in each animal group. (d) The coefficient of
348 variance (CV) of capillary RBC flux across cortical layers II/III and IV, and subcortical white matter in sedentary
349 and exercise group. (e) Venular flow versus vessel diameter. Different symbols represent different animals. The
350 red dashed and blue solid line is the best fit result of each linear regression for sedentary and exercise group,
351 respectively. (f) Mean venular flow in ascending venules in (d) in sedentary and exercise group. The data in (b-d)
352 are from 921, 486, and 112 capillaries in 7 mice in the sedentary group and 1046, 465, and 238 capillaries in 8
353 mice in the exercise group, in cortical layers II/III, IV, and the white matter, respectively. The data in (e) and (f)
354 are from 14 and 7 ascending venules in 9 and 6 mice in the sedentary and exercise group, respectively. Statistical
355 analysis was carried out using Two-way ANOVA with post hoc Tukey's in (a,b) and (d) and Student's t-test in
356 (f). * $p < 0.05$; ** $p < 0.01$. Additional details on boxplots and animals excluded from the analyses are provided in
357 the Supplementary document.

358 *3.2 Aging-induced reduced microvascular oxygenation in deeper cortical regions was rescued by 5-months of* 359 *voluntary exercise*

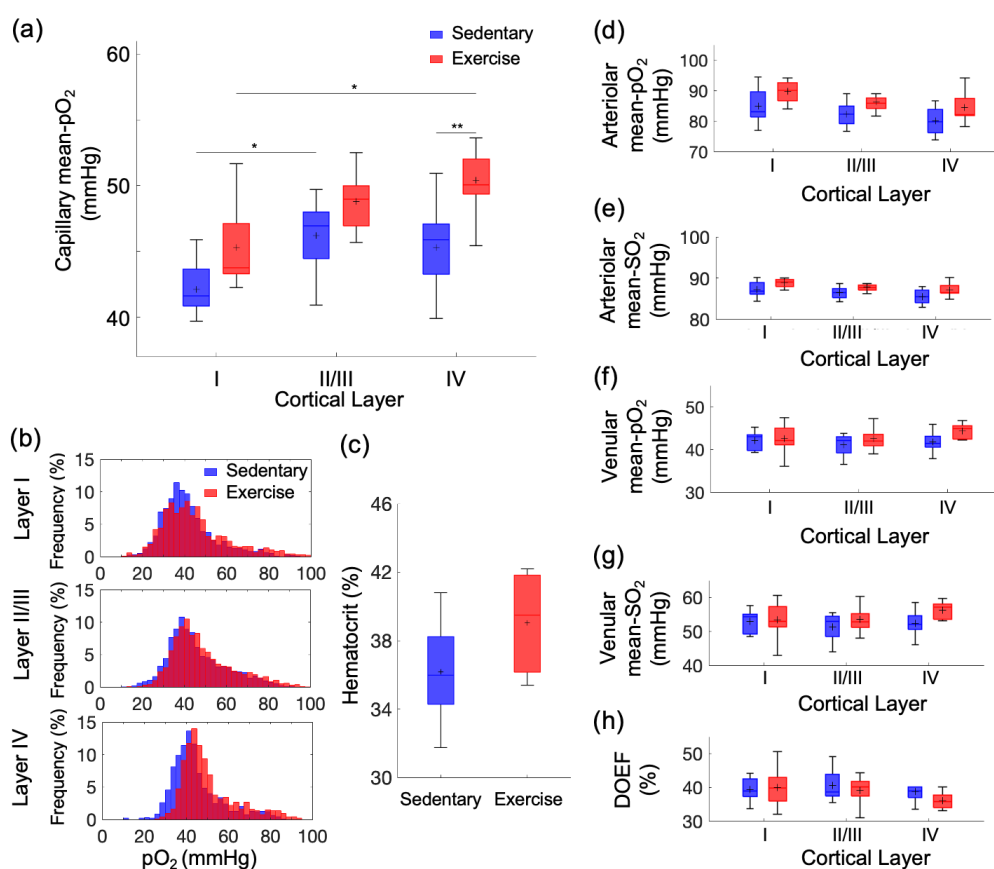
360 We next asked whether aging and exercise-induced changes in capillary RBC flux affected the microvascular
361 oxygenation as well. We performed two-photon phosphorescence lifetime imaging using our two-photon
362 microscope and a phosphorescent oxygen-sensitive probe (Oxyphor 2P) to examine variations of capillary mean
363 pO_2 in both sedentary and exercise group as a function of cortical depth (Figure 4a). We have previously shown
364 that the resting-state capillary mean pO_2 gradually increased from layer I to IV by ~ 6 mmHg in young-adult mice
365 (3-5 months old) of the same strain and sex.(Li et al., n.d.) In contrast, the aged sedentary mice here exhibited a
366 different pattern, with the capillary mean pO_2 reaching a plateau in layers II/III (capillary mean pO_2 , layer I: 42 ± 1
367 mmHg, layers II/III: 46 ± 1 mmHg, layer IV: 45 ± 2 mmHg).

368 The exercise group showed an overall increase in capillary mean- pO_2 in comparison with the sedentary
369 group across all cortical layers (Figure 4a). The pO_2 increase in cortical layer IV was more pronounced compared
370 to the other layers. The distribution of capillary pO_2 in the exercise group also shifted towards higher pO_2
371 compared with sedentary controls (Figure 4b), which was again more pronounced in layer IV. Consistent with our
372 previous report,(Li et al., n.d.) we also found a strong positive correlation between the mean pO_2 and mean

373 capillary RBC flux in both groups (Figure 4 – Figure supplement 1).

374 The increase in the capillary pO_2 could be in part due to an increase in Hct level due to exercise.(Moeini
 375 et al., 2020) We observed a moderate but statistically insignificant increase in Hct in the exercise group compared
 376 with sedentary mice (Figure 4c). No difference in the capillary RBC line-density between two groups was found
 377 (Figure 3 – Figure supplement 2). No correlation between the measured parameters (mean pO_2 and Hct) and the
 378 average daily running distance was found (data not shown).

379 The pO_2 and SO_2 in the diving cortical arterioles and ascending venules across cortical layers were
 380 lower in the old sedentary mice (Figure 4d-g) than what we have reported in young adult mice,(Li et al., n.d.) and
 381 in agreement with the pO_2 values in old mice previously reported by others.(Moeini et al., 2018) Importantly, both
 382 pO_2 and SO_2 tended to increase in all cortical layers in exercise group compared with sedentary group, particularly
 383 in layer IV, consistent with the largest changes in the capillary RBC flux and mean pO_2 observed in the deeper
 384 cortical layers. Consequently, the depth-dependent oxygen extraction fraction (DOEF) decreased in the exercise
 385 group compared with the sedentary controls, with potentially the largest decrease in the layer IV (Figure 4h).

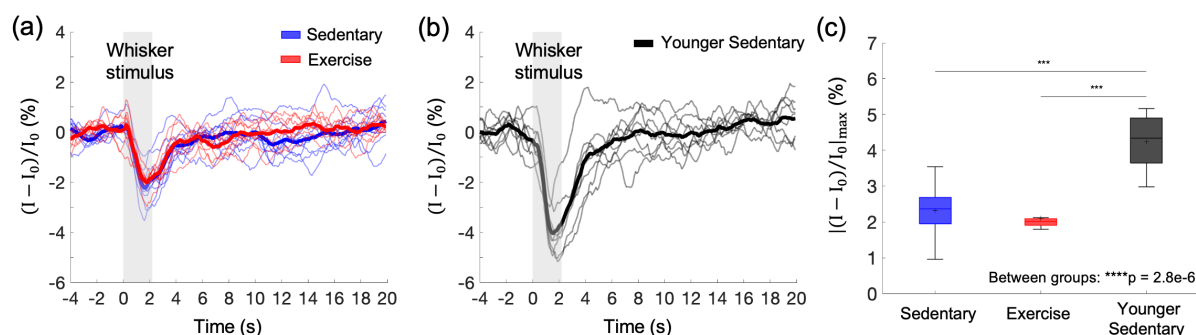


386

387 [Figure 4] Exercise-induced changes in microvascular pO_2 across cortical layers in old mice. (a) Capillary mean-
388 pO_2 across cortical layers in sedentary controls and exercising mice. (b) Histograms of capillary pO_2 in layers I,
389 II/III, and IV. (c) The mean Hct levels from sedentary (n=8) and exercise group (n=5). (d) and (e) Intravascular
390 pO_2 and SO_2 in the diving arterioles across cortical layers I-IV in sedentary (blue boxplots) and exercise (red
391 boxplots) group, respectively. (f) and (g) Intravascular pO_2 and SO_2 in the surfacing venules across cortical layers
392 I-IV in sedentary (blue boxplots) and exercise (red boxplots) group, respectively. (h) Depth-dependent OEF in
393 sedentary (blue boxplots) and exercise (red boxplots) group. The analysis in (a) and (b) was made with 1224,
394 2601, and 922 capillaries across n=9 mice in sedentary group and 1334, 2840, and 1078 capillaries across n=9
395 mice in exercise group in cortical layers, I, II/III, and IV, respectively. The analysis in (d-h) was made with 13
396 arterioles and 12 venules from n=9 mice in sedentary group and 14 arterioles and 12 venules from n=9 mice in
397 exercise group. Statistical analysis was carried out using Two-way ANOVA with post hoc Tukey's in (a) and (d-
398 h) and Student's t-test in (f). * $p < 0.05$; ** $p < 0.01$. Additional details on boxplots and exclusions are provided in
399 the Supplementary document.

400 3.3 Cortical hemodynamic response to functional activation was reduced by aging but not altered by exercise

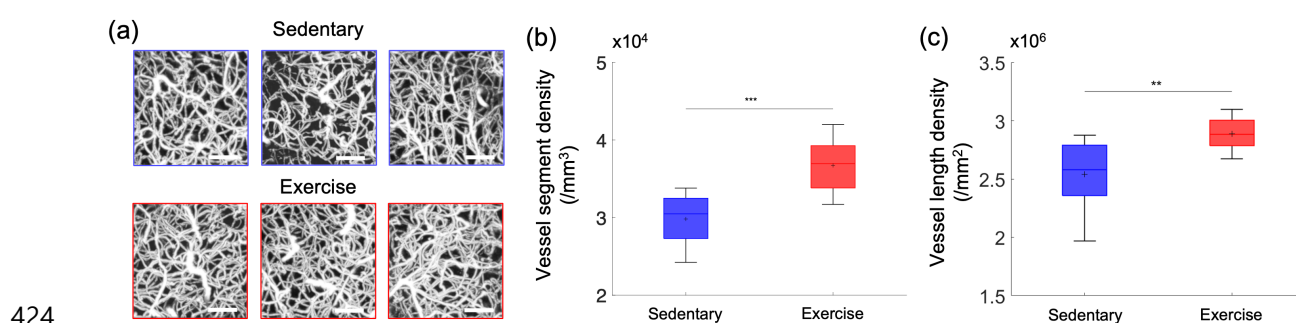
401 The subtle impact of exercise on the gray matter microvascular perfusion and oxygenation led us to question
402 whether it has effects on cortical hemodynamic response. We assessed the effects of aging and exercise on the
403 hemodynamic response to the whisker stimulation using OISI (Figure 5). Optical intrinsic signal time courses of
404 mice in the exercise and sedentary group were obtained (Figure 5a) and compared with those of younger (7 months
405 old) sedentary mice (Figure 5b). The peak amplitudes of the hemodynamic response were significantly smaller in
406 aged mice compared with younger mice regardless of the exercise status (Figure 5c). However, the exercise did
407 not affect the peak response amplitude. Response latency (i.e., time to peak after stimulus onset) also did not differ
408 among the groups (Figure 5 – Figure supplement 1). No correlation between the measured parameters (the peak
409 response amplitude and the response latency) and the average running distance was found (data now shown).



411 [Figure 5] Effects of aging and exercise on functional hemodynamic response. (a, b) Optical intrinsic signal time
412 courses in the whisker barrel cortex of individual old mice in aged sedentary (blue; n=9) and exercise (red; n=8)
413 mice (a), and younger (7 months old) sedentary mice (n=8) (b). Thick curves represent averages. (c) Average
414 changes in the peak intensity in old sedentary, old exercise, and young group. One-way ANOVA with Tukey post
415 hoc test. *** p<0.001. Please see Supplementary document for exclusions.

416 3.4 Cortical microvascular density is significantly larger in the exercise group

417 To explore whether exercise induces structural changes in the cerebral microvasculature of aged mice, we segmented
418 three-dimensional stacks of the cortical microvasculature and obtained their mathematical graph
419 representations. (Tsai et al., 2009) Representative maximum intensity projection (MIP) images of the
420 microvascular stacks show denser cortical microvascular networks of mice from the exercise group compared to
421 those of the sedentary controls (Figure 6a). Exercise group had significantly higher microvascular segment and
422 length density compared with their sedentary controls (Figure 6b, c). Segment and length density did not correlate
423 with running activity (data not shown).

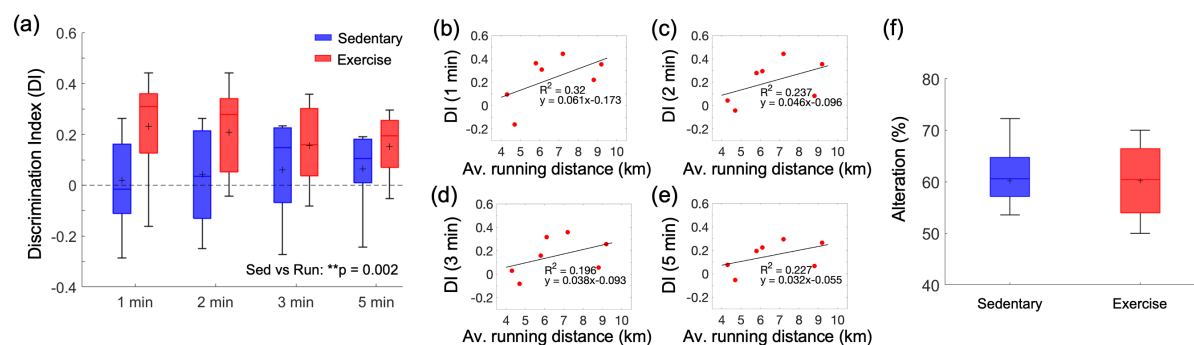


425 [Figure 6] Cortical microvascular density in aged mice. (a) Representative MIP images of the three-dimensional
426 angiograms of three mice in the sedentary group and three mice in the exercise group, over the cortical depth
427 range from 50 μm to 400 μm , and $200 \times 200 \mu\text{m}^2$ FOV. Scale bars: 50 μm . (b) Vessel segment density and (c)
428 vessel length density of cortical capillaries from sedentary (n=19,669 segments; n=9 mice) and exercise (n=18,044
429 segments; n=8 mice) group. Student's t-test. **p<0.01; *** p<0.001. Please see Supplementary document for
430 exclusions.

431 3.5 Exercise improves short-term spatial memory performance

432 In the novel object recognition test, mice from the exercise group spent more time exploring the novel object than
433 the familiar one leading to significantly higher DI scores across four different time intervals than sedentary mice

434 (Figure 7a). Interestingly, the DI score for each time interval correlated with the average daily running distance
435 (Figure 7b-e). In contrast, sedentary and exercise groups did not differ in the Y-maze test performance (Figure
436 7f).



437 [Figure 7] Effect of exercise in the old mice on cognitive performance. (a) DI scores in NORT, calculated with
438 four different exploration time periods in the sedentary (n=9) and exercise (n=7) group. The calculated DI values
439 at each time interval were subsequently averaged across animals. (b-d) Correlations between the daily average
440 running distance and four different DI scores: 1, 2, 3, and 4 minutes, respectively. (f) Spontaneous alteration scores
441 in the Y-maze test in the sedentary (n=9) and exercise (n=7) group. Statistical analysis was carried out using Two-
442 way ANOVA with post hoc Tukey's in (a) and Student's t-test in (f). **p<0.01. Please see Supplementary
443 document for exclusions.
444

445

446 **4. Discussion**

447 In this study, we observed depth-dependent decreases in cerebral microvascular perfusion and oxygenation in
448 aged sedentary mice. The decrease was mitigated by five months of exercise in a depth-dependent manner. The
449 key findings include (1) age-associated reduction in capillary RBC flux in the white matter that was moderated
450 by exercise; (2) a decrease in the mean capillary pO₂ in cortical layer IV with aging and the overall improvement
451 in capillary pO₂ with exercise, with a particularly pronounced pO₂ increase in layer IV; (3) an increase in cortical
452 microvascular density with exercise; and (4) improvement of short-term memory function with exercise.

453 We first assessed the spatial distribution of capillary RBC flux across the cortical and subcortical regions
454 and how it responds to aging and exercise. In aged sedentary mice, the capillary RBC flux in the subcortical white
455 matter tended to be lower than that in the gray matter (Figure 3b). Young adult sedentary mice showed the opposite
456 trend (Figure 3a), consistent with our previous finding in anesthetized young adult mice (3-5 months old) showing
457 a higher capillary RBC flux in the subcortical white matter compared to the gray matter.(Li et al., 2020)
458 Importantly, we observed a large discrepancy in the capillary RBC flux between young and aged sedentary mice
459 in the gray matter and an almost two-fold greater RBC flux discrepancy between the two groups in the white
460 matter. Cerebral white matter is known to be more susceptible to hypoperfusion compared to the gray matter,
461 potentially because it is located further downstream with respect to the arterial blood supply.(Gunning-Dixon et
462 al., 2009; Markus et al., 2000) White matter vulnerability to ischemic injury increases with age,(Baltan et al., 2008)
463 and white matter lesions and lacunar infarcts are common in elderly people with CSVD and hypertension.(Breteler
464 et al., 1994; van Swieten et al., 1991) The vulnerability of white matter to such pathological conditions could be
465 related to our observation of a severe decrease in blood flow in the white matter during normal aging.

466 Five months of exercise restored the spatial distribution trend of capillary RBC flux close to its
467 distribution in the young sedentary mice (Figure 3b). Increased capillary perfusion in the white matter was
468 associated with increased blood flow in ascending venules, as measured by Doppler OCT (Figure 3e,f). In contrast
469 to smaller ascending venules having their branches being distributed mostly over the upper cortical layers, large
470 venules likely extend further to subcortical white matter where the increased capillary perfusion was
471 observed.(Duvernoy et al., 1981; Kirst et al., 2020; Xiong et al., 2017) Venules smaller than 20 μm in diameter
472 were excluded from analysis as the small venules tend to have slower flow and may have smaller absolute changes
473 in the blood flow compared to larger venules with higher flow and thus the flow change may not be easily
474 distinguishable due to the relatively low precision of the speed measurement based on Doppler OCT (± 0.7 mm/s,

475 see *Methods 2.4* for more details).(Fan et al., 2020; Santisakultarm et al., 2012)

476 Previous studies in mice reported conflicting results regarding the effects of exercise on cortical
477 microcirculation.(Dorr et al., 2017; Falkenhain et al., 2020; Lu et al., 2020) However, these observations have
478 been limited to the blood flow in gray matter, which was shown in this study to be less responsive to exercise than
479 that in deeper brain regions. Human MRI data acquired after short-term (one week) exercise showed that exercise
480 induced a selective increase in hippocampal CBF with no or negligible changes in the gray matter CBF.(Steventon
481 et al., 2021) Our findings suggest that cerebral subcortical microcirculation is more responsive to both age-related
482 and exercise-induced changes than cortical microcirculation.

483 The change in cortical microvascular oxygenation was also depth-dependent. In aged sedentary mice,
484 the mean capillary pO₂ increased from layer I to layer II/III and reached a plateau in layer II/III (Figure 5a, b). A
485 different trend was observed in young sedentary mice, which showed a gradual increase in the mean capillary pO₂
486 from layer I to layer IV.(Li et al., n.d.) In contrast to aged sedentary controls, mice from the exercise group showed
487 a similar trend to young sedentary mice, with a pronounced increase in the mean capillary pO₂ in layer IV among
488 all assessed cortical layers. In the mouse somatosensory cortex, layer IV exhibits the highest neuronal and
489 capillary densities and the strongest staining for the cytochrome c oxidase, potentially implying the highest
490 oxidative demand during activation and/or at rest throughout all cortical layers.(Blinder et al., 2013; Lefort et al.,
491 2009) In an immunohistochemical study performed using an anti-Glut-1 antibody, high plaque load and decreased
492 blood vessel density were observed, particularly in layer IV of the somatosensory cortex in aged, 18-month-old
493 transgenic AD mice, while younger AD mice did not demonstrate any difference compared to the wild-type
494 mice.(Kuznetsova & Schliebs, 2013) The decrease in capillary mean pO₂ in layer IV in aged sedentary mice could
495 be associated with the larger mismatch in the oxygen delivery and consumption compared with the more
496 superficial cortical layers. However, due to technical limitations, we did not assess the microvascular oxygenation
497 in the deeper cortical layers and subcortical white matter. Because RBC flux exhibits the largest discrepancy
498 between sedentary old and young mice in the subcortical white matter, it is possible that intravascular pO₂ also
499 exhibits the largest discrepancy in this brain region.

500 Voluntary exercise significantly improved microvascular oxygenation compared to sedentary controls,
501 particularly in layer IV. Similar to our finding of capillary RBC flux improvement due to exercise mostly in the
502 white matter, exercise differentially affected cortical intravascular oxygenation, with the largest increase in the
503 deeper layers and restored the spatial distribution trend of capillary pO₂ across cortical layers close to its

504 distribution in the young sedentary mice. However, since the difference in both the Hct level and RBC line density
505 between the two groups was not significant (Figure 5c and Figure 3 – Figure supplement 2), factors other than
506 increased Hct may be involved in the observed depth-dependent pO_2 increase in the gray matter. Interestingly, we
507 found that the RBC line density in both groups of aged mice was significantly higher in the subcortical white
508 matter than in the gray matter. This was not observed in young adult mice.(Li et al., 2020) However, this finding
509 is consistent with previous simulation results that showed higher Hct levels in deep-reaching penetrating arterioles
510 compared to arterioles whose branches connect to the capillary bed closer to the surface due to the plasma
511 skimming effect.(Gould et al., 2017)

512 We observed no change in the relative peak amplitude or the latency of stimulus-induced hemodynamic
513 response with exercise, assessed with OISI at 570 nm, which emphasizes the intrinsic signal originating from
514 cerebral blood volume changes in the superficial cortical layers (Figure 5 and Figure 5 – Figure supplement
515 1).(Malonek et al., 1997; Tian et al., 2011) Young sedentary mice (7 months old) showed a significantly larger
516 relative response amplitude than aged mice, consistent with the reduced cerebrovascular reactivity with age in
517 healthy adults and rodents.(Bálint et al., 2019; J. N. Barnes, 2015; Seker et al., 2021) The baseline CBF can have
518 a strong effect on the magnitude of the hemodynamic response.(Buxton et al., 2004; Corfield et al., 2001) While
519 no statistically significant difference in the mean capillary RBC flux in the gray matter was found between the
520 aged sedentary and exercise group (Figure 3b), the exercise group had larger capillary density in the gray matter
521 (Figure 6b), suggesting that cortical blood perfusion was possibly also higher in the exercise group. This was
522 further supported by significantly higher blood flow in ascending venules in the same group (Figures 3e,f).
523 Therefore, our data implies that with a similar level of the relative response amplitude between two groups, the
524 exercise group potentially had a larger transient blood supply to the tissue during functional hyperemia.

525 Increased capillary density in the sensorimotor cortex and hippocampus in response to exercise has been
526 observed in both old rats and young adult mice.(Ding et al., 2006; Morland et al., 2017) However, other studies
527 showed no improvement in cerebral microvascular structure with regular exercise in the sensorimotor cortex of
528 mice of a similar age range.(Dorr et al., 2017; Falkenhain et al., 2020) Although it is unclear whether the difference
529 in age or brain region (or both) contributed to the inconsistent results with some of the previous observations, we
530 found significant morphological changes in the microvascular morphometric parameters due to chronic exercise
531 in the somatosensory cortex of 20-month-old mice (Figure 6). Based on the observed changes in the microvascular
532 RBC flux and pO_2 , we anticipate that an even greater discrepancy in the capillary density between the two groups

533 of mice may be observed in deeper cortical layers and subcortical white matter. It is compelling to hypothesize
534 that higher microvascular density is one of the major contributors to the larger microvascular perfusion and
535 oxygenation observed in mice from the exercise group. However, it is not clear whether the larger capillary density
536 in the exercise group is mostly due to increased angiogenesis or decreased pruning of the capillaries in comparison
537 with the sedentary group. In addition, if increased angiogenesis is present in the exercise group, it will be important
538 to better understand the contribution of the new capillaries to oxygen delivery to tissue.

539 Increased cerebral perfusion and oxygenation with exercise were accompanied by improved spatial
540 short-term memory function, as evaluated by NORT (Figure 7a). The perirhinal cortex plays an important role in
541 object recognition memory. It receives sensory inputs from its neighboring sensory cortices, such as the
542 somatosensory cortex, where we found significant improvements in vascular function and structure due to exercise
543 in aged mice.(Antunes & Biala, 2012; Cohen & Stackman Jr., 2015) In contrast, we did not observe an increase
544 in spontaneous alterations between the arms of the Y-maze (Figure 7c). As previously shown in several studies in
545 mouse models of AD, each memory task depends on a variety of brain regions that can be differentially affected
546 by exercise, which could potentially produce inconsistent results between different memory tasks.(Kraeuter et al.,
547 2019; Winters, 2004) The NORT results depend on the exploration time in the test phase, which is related to the
548 age-dependent decay of the novel object preference.(Traschütz et al., 2018) Therefore, choosing an adequate time
549 interval to calculate the discrimination index is important to reliably detect novel object recognition, especially in
550 aged mice. In our analysis, the DI score was calculated at four different time intervals: 1, 2, 3, and 5 min. The
551 results showed an increased DI score in running mice compared to sedentary mice across all time intervals, which
552 was also positively correlated with the average running distance (Figure 7b).

553 A recent study reported a positive correlation between the average daily running distance and cerebral
554 tissue oxygenation in 6-month-old mice after three months of exercise.(Lu et al., 2020) While mice in our exercise
555 group had significantly higher white matter capillary RBC flux than sedentary mice, the mean capillary RBC flux
556 in the white matter was negatively correlated with the average daily running distance (Figure 3 – Figure
557 supplement 3). Although white matter capillary density was not assessed in this study, lower capillary RBC flux
558 in the white matter could potentially be accompanied with higher capillary density. In this case, capillary RBC
559 flux in the white matter can decrease but cerebral tissue oxygenation in this region can still increase in response
560 to chronic exercise. This result also may be due to a non-proportional relationship between exercise and brain
561 function, which could decrease after reaching the optimal intensity of exercise.(Khakroo Abkenar et al., 2019) It

562 is possible that five months of unrestricted exercise led some (or all) animals to over-exercise, which may
563 adversely affect subcortical capillary blood flow and prevent achieving the maximum benefits of exercise on the
564 microcirculation.

565 In the analysis of the capillary RBC flux and capillary pO_2 , all capillaries identified within the FOV
566 were selected and used for analysis without considering their branching orders. In future studies, analysis based
567 on different types of vessels classified by branching order could potentially provide additional insight into
568 capillary blood flow and oxygenation, as we previously showed different characteristics of capillaries with low
569 branching orders located close to precapillary arterioles compared with higher-order capillaries.(Li et al., n.d.)

570 In conclusion, leveraging our multimodal optical imaging tools, we quantified the changes in
571 microvascular function, structure, and sensory-evoked functional hyperemia in response to aging and voluntary
572 exercise in 20-month-old mice. Our results indicate that cerebral microcirculation and oxygenation in deeper
573 cortical layers and subcortical white matter are more susceptible to age-related degeneration, but they are
574 surprisingly more responsive to voluntary aerobic exercise, which induces significant improvements in capillary
575 density, RBC flux, and intracapillary pO_2 . Improvements in cerebrovascular function and structure are
576 accompanied by rescue of cognitive function. These findings may help us to better understand the patterns and
577 consequences of age-related decline of microcirculation at different cortical depths and subcortical white matter,
578 and how the neurologic effects of aging may be ameliorated by aerobic exercise.

579

580 **5. Acknowledgements**

581 Support of the grants RF1NS121095, R01NS115401, U24EB028941, U19NS123717, U01HL133362,
582 R00MH120053, and R01AG055413 from the National Institutes of Health, USA, and support from the Rappaport
583 Foundation and Leducq Foundation are gratefully acknowledged. The funders had no role in study design, data
584 collection and interpretation, or the decision to submit the work for publication.

585

586 **6. Competing interests**

587 The authors declare no competing interests.

588

589

590 **[Source Files]**

591 **Figure3_SourceData1**

592 Capillary RBC flux measured in young sedentary mice

593 **Figure3_Source Data2**

594 Capillary RBC flux measured in aged mice

595 **Figure3_Source Data3**

596 Venous flow measured in aged mice

597 **Figure4_Source Data1**

598 Capillary Po₂ measured in aged mice

599 **Figure4_Source Data2**

600 Blood hematocrit level

601 **Figure4_Source Data3**

602 Arterial (and venous) Po₂ measured in aged mice

603 **Figure5_Source Data1**

604 Peak hemodynamic response amplitude measured in aged mice

605 **Figure6_Source Data1**

606 Cortical capillary segment/length density measured in aged mice

607 **Figure7_Source Data1**

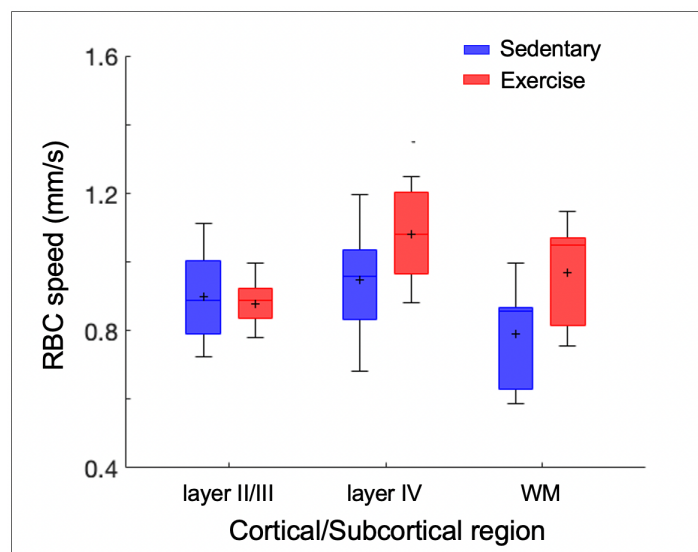
608 Behavioral scores from NORT and Y-maze test

609

610

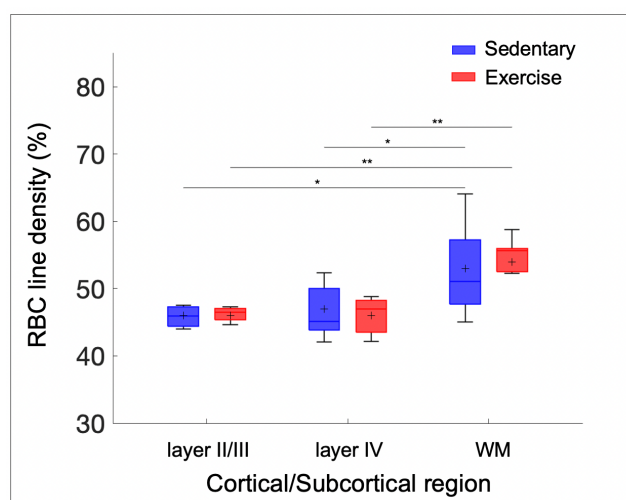
611

612 [Supplementary Figures]



613

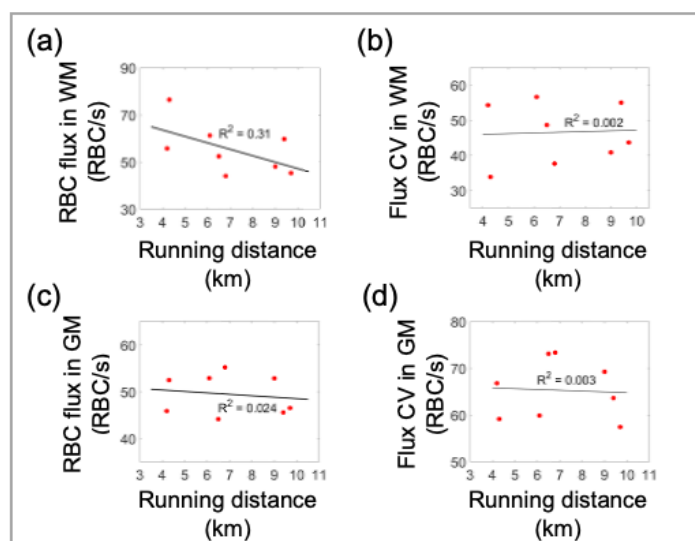
614 [Figure 3 – Figure supplement 1] Exercise induced alterations in capillary RBC speed. Capillary RBC speed across
615 cortical layers II/III and IV, and subcortical white matter in aged sedentary and running mice, respectively. The
616 analysis was made with 921, 486, and 112 capillaries across n=7 mice in the sedentary group and 1046, 465, and
617 238 capillaries across n=8 mice in the exercise group in cortical layers, II/III, IV, and the white matter. Statistical
618 comparisons were carried out using Two-way ANOVA with Tukey post hoc test.



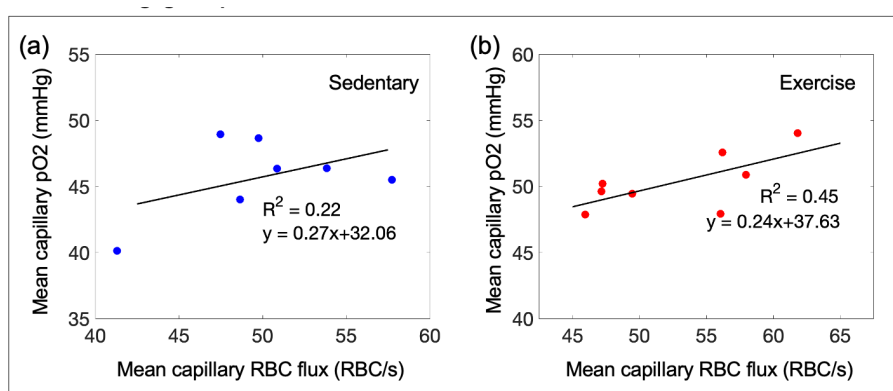
619

620 [Figure 3 – Figure supplement 2] Exercise induced alterations in capillary RBC line-density. Capillary RBC line-
621 density across cortical layers II/III and IV, and subcortical white matter in aged sedentary and running mice. The
622 analysis was made with 921, 486, and 112 capillaries across n=7 mice in sedentary group and 1046, 465, and 238
623 capillaries across n=8 mice in the exercise group in cortical layers, II/III, IV, and the white matter. Statistical

624 comparisons were carried out using Two-way ANOVA with Tukey post hoc test. The single-asterisk symbol (*)
625 indicates $p < 0.05$; the double-asterisk symbol (**) indicates $p < 0.01$.

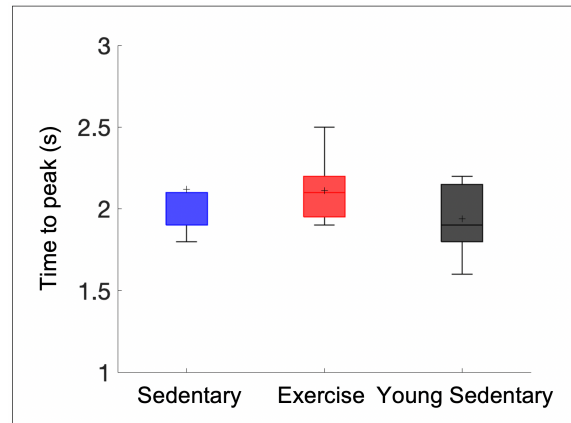


627 [Figure 3 – Figure supplement 3] Correlations between the capillary RBC flux and CV, and the running activity.
628 Each data point represents an individual animal. The black solid line is the best linear regression fit. (a) and (b)
629 Correlations between the capillary RBC flux and CV in the white matter and the average daily running distance,
630 respectively. (c) and (d) Correlations between the CV of capillary RBC flux and CV in the gray matter and the
631 average daily running distance, respectively. For each animal, the gray matter capillary RBC flux was calculated
632 by averaging the acquired flux values from cortical layers II/III and IV.



634 [Figure 4 – Figure supplement 1] Capillary mean- pO_2 vs capillary RBC flux in the mouse cortex. (a) and (b)
635 Correlations between the mean capillary pO_2 and the mean capillary RBC flux in sedentary and running mice,
636 respectively. The black solid line is the best fit result of each linear regression ($R^2 = 0.22, y = 0.27x + 32.06$,
637 for sedentary mice and $R^2 = 0.45, y = 0.24x + 37.63$, for running mice). Each data point represents an

638 individual animal. For each animal, the mean capillary RBC flux and the mean capillary pO_2 were calculated by
639 averaging the acquired RBC flux and pO_2 values from cortical layers II/III and IV, and cortical layers I, II/III, and
640 IV, respectively. The correlation coefficient (the R value) for each group was converted to Fisher z value to
641 compare difference between correlation coefficients of sedentary and running mice, and no significant difference
642 was found (the observed z value = 0.44).



643

644 [Figure 5 – Figure supplement 1 Differences in the latency (time to peak) of stimulus-induced hemodynamic
645 response between sedentary, running, and younger mice. Statistical comparisons were carried out using One-way
646 ANOVA with Tukey post hoc test.

647

648 **5. Reference**

- 649 Antunes, M., & Biala, G. (2012). The novel object recognition memory: neurobiology, test procedure, and its
650 modifications. *Cognitive Processing*, *13*(2), 93–110. <https://doi.org/10.1007/s10339-011-0430-z>
- 651 Bálint, A. R., Puskás, T., Menyhárt, Á., Kozák, G., Szenti, I., Kónya, Z., Marek, T., Bari, F., & Farkas, E. (2019).
652 Aging Impairs Cerebrovascular Reactivity at Preserved Resting Cerebral Arteriolar Tone and Vascular
653 Density in the Laboratory Rat. *Frontiers in Aging Neuroscience*, *11*.
654 <https://doi.org/10.3389/fnagi.2019.00301>
- 655 Baltan, S., Besancon, E. F., Mbow, B., Ye, Z., Hamner, M. A., & Ransom, B. R. (2008). White Matter Vulnerability
656 to Ischemic Injury Increases with Age Because of Enhanced Excitotoxicity. *Journal of Neuroscience*, *28*(6),
657 1479–1489. <https://doi.org/10.1523/JNEUROSCI.5137-07.2008>
- 658 Barnes, D. E., Yaffe, K., Satariano, W. A., & Tager, I. B. (2003). A Longitudinal Study of Cardiorespiratory Fitness
659 and Cognitive Function in Healthy Older Adults. *JAGS*, *51*, 459–465.
- 660 Barnes, J. N. (2015). Exercise, cognitive function, and aging. *Advances in Physiology Education*, *39*(2), 55–62.
661 <https://doi.org/10.1152/advan.00101.2014>
- 662 Blinder, P., Tsai, P. S., Kaufhold, J. P., Knutsen, P. M., Suhl, H., & Kleinfeld, D. (2013). The cortical angiome: An
663 interconnected vascular network with noncolumnar patterns of blood flow. *Nature Neuroscience*, *16*(7),
664 889–897. <https://doi.org/10.1038/nn.3426>
- 665 Breteler, M. M. B., van Swieten, J. C., Bots, M. L., Grobbee, D. E., Claus, J. J., van den Hout, J. H. W., van
666 Harskamp, F., Tanghe, H. L. J., de Jong, P. T. V. M., van Gijn, J., & Hofman, A. (1994). Cerebral white
667 matter lesions, vascular risk factors, and cognitive function in a population-based study. *Neurology*, *44*(7),
668 1246–1246. <https://doi.org/10.1212/WNL.44.7.1246>
- 669 Buxton, R. B., Uludağ, K., Dubowitz, D. J., & Liu, T. T. (2004). Modeling the hemodynamic response to brain
670 activation. *NeuroImage*, *23*, S220–S233. <https://doi.org/10.1016/j.neuroimage.2004.07.013>
- 671 Cees De Groot, J., de Leeuw, F.-E., Oudkerk, M., van Gijn, J., Hofman, A., Jolles, J., & Breteler, M. M. B. (2000).
672 Cerebral White Matter Lesions and Cognitive Function: The Rotterdam Scan Study. *Annals of Neurology*,
673 *47*, 145–157.

- 674 Cohen, S. J., & Stackman Jr., R. W. (2015). Assessing rodent hippocampal involvement in the novel object
675 recognition task. A review. *Behavioural Brain Research*, 285, 105–117.
676 <https://doi.org/10.1016/j.bbr.2014.08.002>
- 677 Corfield, D. R., Murphy, K., Josephs, O., Adams, L., & Turner, R. (2001). Does Hypercapnia-Induced Cerebral
678 Vasodilation Modulate the Hemodynamic Response to Neural Activation? *NeuroImage*, 13(6), 1207–1211.
679 <https://doi.org/10.1006/nimg.2001.0760>
- 680 de Leeuw, F. E., de Groot, J. C., Achten, E., Oudkerk, M., Ramos, L. M. P., Heijboer, R., Hofman, A., Jolles, J.,
681 van Gijn, J., & Breteler, M. M. B. (2001). Prevalence of cerebral white matter lesions in elderly people: A
682 population based magnetic resonance imaging study. The Rotterdam Scan Study. *Journal of Neurology*
683 *Neurosurgery and Psychiatry*, 70(1), 9–14. <https://doi.org/10.1136/jnnp.70.1.9>
- 684 de Miguel, Z., Khoury, N., Betley, M. J., Lehallier, B., Willoughby, D., Olsson, N., Yang, A. C., Hahn, O., Lu, N.,
685 Vest, R. T., Bonanno, L. N., Yerra, L., Zhang, L., Saw, N. L., Fairchild, J. K., Lee, D., Zhang, H., McAlpine,
686 P. L., Contrepois, K., ... Wyss-Coray, T. (2021). Exercise plasma boosts memory and dampens brain
687 inflammation via clusterin. *Nature*, 600(7889), 494–499. <https://doi.org/10.1038/s41586-021-04183-x>
- 688 Defrancesco, M., Egger, K., Marksteiner, J., Esterhammer, R., Hinterhuber, H., Deisenhammer, E. A., & Schocke,
689 M. (2014). Changes in white matter integrity before conversion from mild cognitive impairment to
690 Alzheimer's disease. *PLoS ONE*, 9(8). <https://doi.org/10.1371/journal.pone.0106062>
- 691 Ding, Y.-H., Li, J., Zhou, Y., Rafols, J., Clark, J., & Ding, Y. (2006). Cerebral Angiogenesis and Expression of
692 Angiogenic Factors in Aging Rats after Exercise. *Current Neurovascular Research*, 3(1), 15–23.
693 <https://doi.org/10.2174/156720206775541787>
- 694 Dorr, A., Thomason, L. A., Koletar, M. M., Joo, I. L., Steinman, J., Cahill, L. S., Sled, J. G., & Stefanovic, B.
695 (2017). Effects of voluntary exercise on structure and function of cortical microvasculature. *Journal of*
696 *Cerebral Blood Flow and Metabolism*, 37(3), 1046–1059. <https://doi.org/10.1177/0271678X16669514>
- 697 Duvernoy, H. M., Delon, S., & Vannson, J. L. (1981). Cortical blood vessels of the human brain. *Brain Research*
698 *Bulletin*, 7(5), 519–579. [https://doi.org/10.1016/0361-9230\(81\)90007-1](https://doi.org/10.1016/0361-9230(81)90007-1)
- 699 Esipova, T. v., Barrett, M. J. P., Erlebach, E., Masunov, A. E., Weber, B., & Vinogradov, S. A. (2019). Oxyphor
700 2P: A High-Performance Probe for Deep-Tissue Longitudinal Oxygen Imaging. *Cell Metabolism*, 29(3),

- 701 736-744.e7. <https://doi.org/10.1016/j.cmet.2018.12.022>
- 702 Esiri, M. M., Nagy, Z., Smith, M. Z., Barnetson, L., Smith, A. D., & Joachim, C. (1999). Cerebrovascular disease
703 and threshold for dementia in the early stages of Alzheimer's disease. *Lancet*, 354(9182), 919–920.
704 [https://doi.org/10.1016/S0140-6736\(99\)02355-7](https://doi.org/10.1016/S0140-6736(99)02355-7)
- 705 Falkenhain, K., Ruiz-Urbe, N. E., Haft-Javaherian, M., Ali, M., Catchers, S., Michelucci, P. E., Schaffer, C. B.,
706 & Bracko, O. (2020). A pilot study investigating the effects of voluntary exercise on capillary stalling and
707 cerebral blood flow in the APP/PS1 mouse model of Alzheimer's disease. *PLoS ONE*, 15(8 August).
708 <https://doi.org/10.1371/journal.pone.0235691>
- 709 Fan, J. L., Rivera, J. A., Sun, W., Peterson, J., Haeberle, H., Rubin, S., & Ji, N. (2020). High-speed volumetric
710 two-photon fluorescence imaging of neurovascular dynamics. *Nature Communications*, 11(1), 6020.
711 <https://doi.org/10.1038/s41467-020-19851-1>
- 712 Gould, I. G., Tsai, P., Kleinfeld, D., & Linninger, A. (2017). The capillary bed offers the largest hemodynamic
713 resistance to the cortical blood supply. *Journal of Cerebral Blood Flow & Metabolism*, 37(1), 52–68.
714 <https://doi.org/10.1177/0271678X16671146>
- 715 Guizar-Sicairos, M., Thurman, S. T., & Fienup, J. R. (2008). Efficient subpixel image registration algorithms. In
716 *OPTICS LETTERS* (Vol. 100, Issue 2).
- 717 Gunning-Dixon, F. M., Brickman, A. M., Cheng, J. C., & Alexopoulos, G. S. (2009). Aging of cerebral white
718 matter: A review of MRI findings. In *International Journal of Geriatric Psychiatry* (Vol. 24, Issue 2, pp.
719 109–117). John Wiley and Sons Ltd. <https://doi.org/10.1002/gps.2087>
- 720 Hase, Y., Ding, R., Harrison, G., Hawthorne, E., King, A., Gettings, S., Platten, C., Stevenson, W., Craggs, L. J.
721 L., & Kalaria, R. N. (2019). White matter capillaries in vascular and neurodegenerative dementias. *Acta*
722 *Neuropathologica Communications*, 7(1), 16. <https://doi.org/10.1186/s40478-019-0666-x>
- 723 Islam, M. R., Valaris, S., Young, M. F., Haley, E. B., Luo, R., Bond, S. F., Mazuera, S., Kitchen, R. R., Caldarone,
724 B. J., Bettio, L. E. B., Christie, B. R., Schmider, A. B., Soberman, R. J., Besnard, A., Jedrychowski, M. P.,
725 Kim, H., Tu, H., Kim, E., Choi, S. H., ... Wrann, C. D. (2021). Exercise hormone irisin is a critical regulator
726 of cognitive function. *Nature Metabolism*, 3(8), 1058–1070. <https://doi.org/10.1038/s42255-021-00438-z>
- 727 Khakroo Abkenar, I., Rahmani-nia, F., & Lombardi, G. (2019). The Effects of Acute and Chronic Aerobic Activity

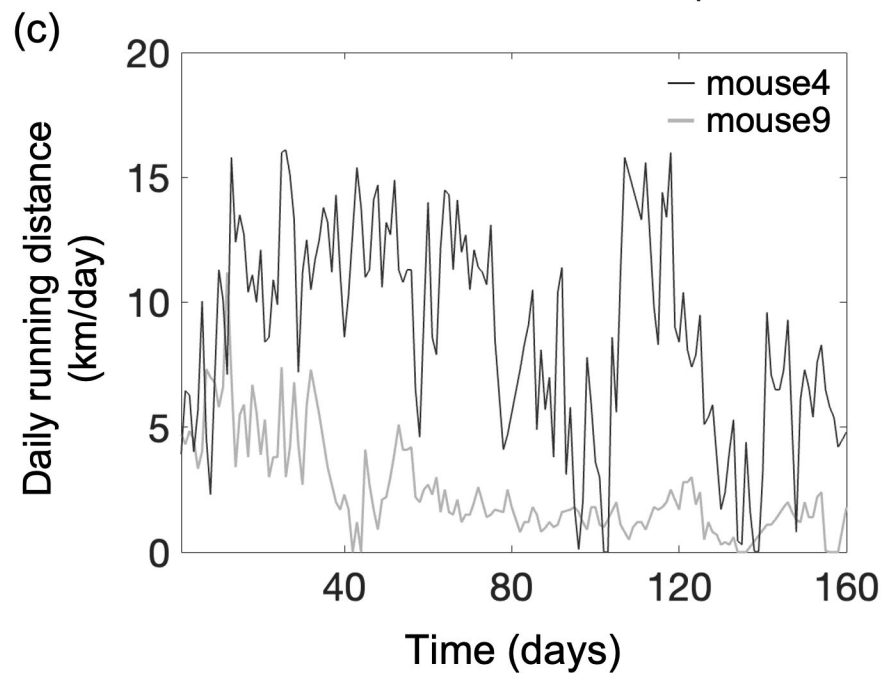
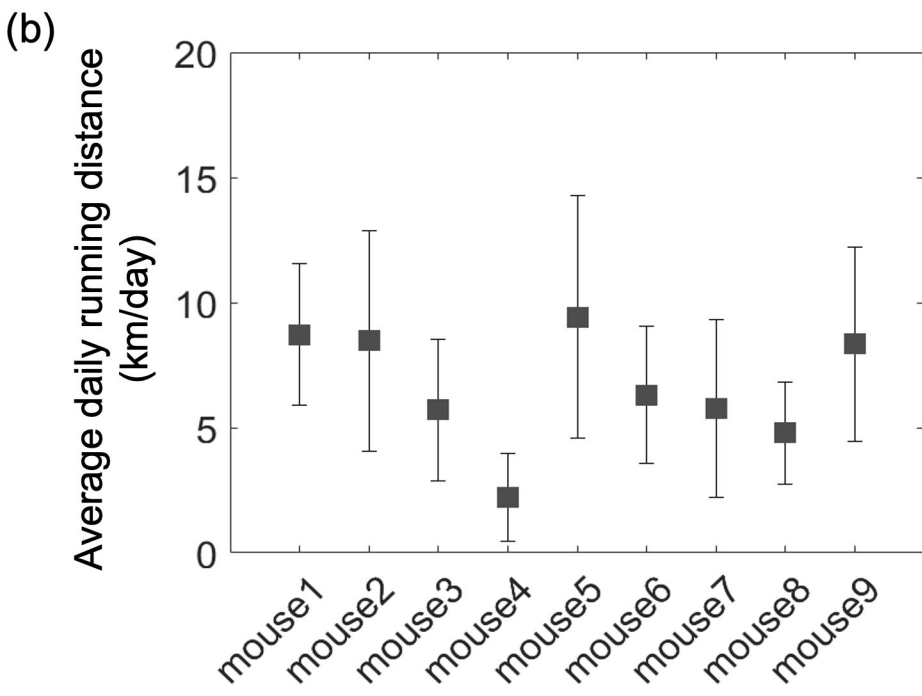
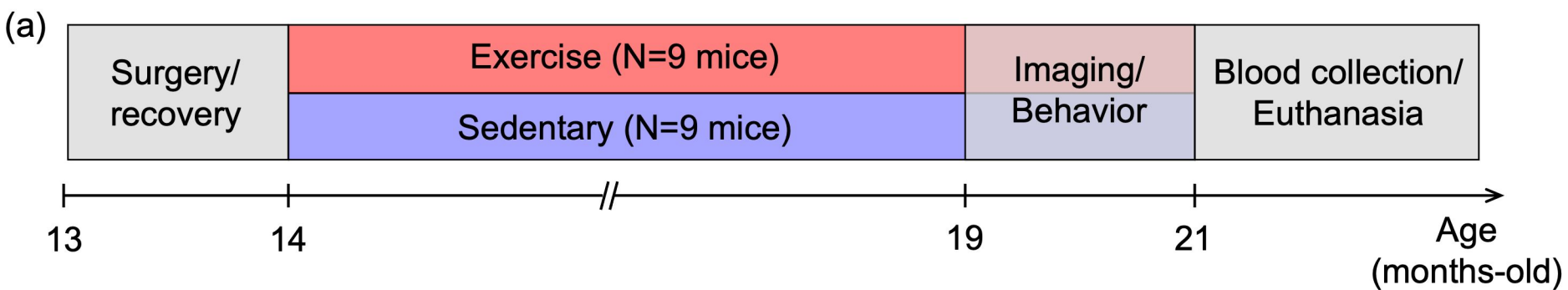
- 728 on the Signaling Pathway of the Inflammasome NLRP3 Complex in Young Men. *Medicina*, 55(4), 105.
729 <https://doi.org/10.3390/medicina55040105>
- 730 Kirst, C., Skriabine, S., Vieites-Prado, A., Topilko, T., Bertin, P., Gerschenfeld, G., Verny, F., Topilko, P., Michalski,
731 N., Tessier-Lavigne, M., & Renier, N. (2020). Mapping the Fine-Scale Organization and Plasticity of the
732 Brain Vasculature. *Cell*, 180(4), 780-795.e25. <https://doi.org/10.1016/j.cell.2020.01.028>
- 733 Koch, E., Walther, J., & Cuevas, M. (2009). Limits of Fourier domain Doppler-OCT at high velocities. *Sensors*
734 *and Actuators, A: Physical*, 156(1), 8–13. <https://doi.org/10.1016/j.sna.2009.01.022>
- 735 Kraeuter, A.-K., Guest, P. C., & Sarnyai, Z. (2019). *The Y-Maze for Assessment of Spatial Working and Reference*
736 *Memory in Mice* (pp. 105–111). https://doi.org/10.1007/978-1-4939-8994-2_10
- 737 Kuznetsova, E., & Schliebs, R. (2013). β -Amyloid, Cholinergic Transmission, and Cerebrovascular System - A
738 Developmental Study in a Mouse Model of Alzheimer's Disease. *Current Pharmaceutical Design*, 19(38),
739 6749–6765. <https://doi.org/10.2174/13816128113199990711>
- 740 Lefort, S., Tomm, C., Floyd Sarria, J. C., & Petersen, C. C. H. (2009). The Excitatory Neuronal Network of the
741 C2 Barrel Column in Mouse Primary Somatosensory Cortex. *Neuron*, 61(2), 301–316.
742 <https://doi.org/10.1016/j.neuron.2008.12.020>
- 743 Li, B., Esipova, T. v, Sencan, I., Kılıç, K., Fu, B., Desjardins, M., Moeini, M., Kura, S., Yaseen, M. A., Lesage, F.,
744 Østergaard, L., Devor, A., Boas, D. A., Vinogradov, S. A., & Sakadž, S. (n.d.). *More homogeneous capillary*
745 *flow and oxygenation in deeper cortical layers correlate with increased oxygen extraction.*
746 <https://doi.org/10.7554/eLife.42299.001>
- 747 Li, B., Ohtomo, R., Thunemann, M., Adams, S. R., Yang, J., Fu, B., Yaseen, M. A., Ran, C., Polimeni, J. R., Boas,
748 D. A., Devor, A., Lo, E. H., Arai, K., & Sakadžić, S. (2020). Two-photon microscopic imaging of capillary
749 red blood cell flux in mouse brain reveals vulnerability of cerebral white matter to hypoperfusion. *Journal*
750 *of Cerebral Blood Flow and Metabolism*, 40(3), 501–512. <https://doi.org/10.1177/0271678X19831016>
- 751 Lu, X., Moeini, M., Li, B., de Montgolfier, O., Lu, Y., Bélanger, S., Thorin, É., & Lesage, F. (2020). Voluntary
752 exercise increases brain tissue oxygenation and spatially homogenizes oxygen delivery in a mouse model
753 of Alzheimer's disease. *Neurobiology of Aging*, 88, 11–23.
754 <https://doi.org/10.1016/j.neurobiolaging.2019.11.015>

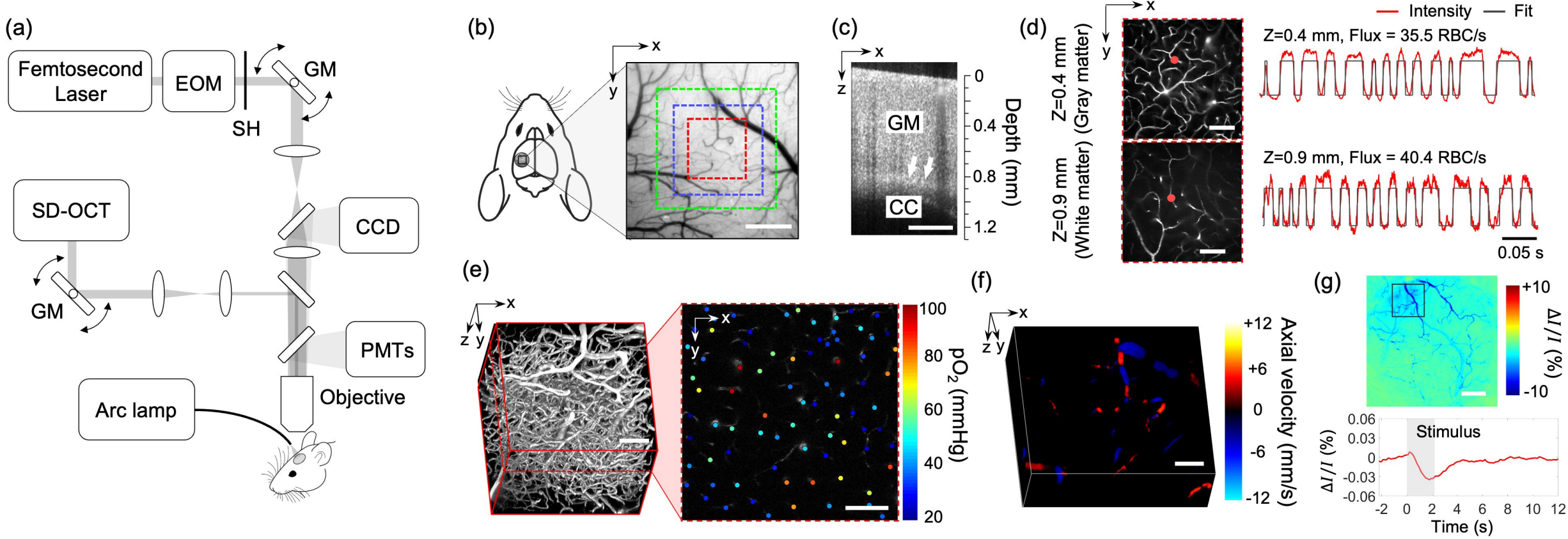
- 755 Malonek, D., Dirnagl, U., Lindauer, U., Yamada, K., Kanno, I., & Grinvald, A. (1997). Vascular imprints of
756 neuronal activity: Relationships between the dynamics of cortical blood flow, oxygenation, and volume
757 changes following sensory stimulation. *Proceedings of the National Academy of Sciences*, *94*(26), 14826–
758 14831. <https://doi.org/10.1073/pnas.94.26.14826>
- 759 Markus, H. S., Lythgoe, D. J., Ostegaard, L., O'sullivan, M., & Williams, C. R. (2000). Reduced cerebral blood
760 flow in white matter in ischaemic leukoaraiosis demonstrated using quantitative exogenous contrast based
761 perfusion MRI. In *J Neurol Neurosurg Psychiatry* (Vol. 69).
- 762 Moeini, M., Cloutier-Tremblay, C., Lu, X., Kakkar, A., & Lesage, F. (2020). Cerebral tissue pO₂ response to
763 treadmill exercise in awake mice. *Scientific Reports*, *10*(1), 13358. [https://doi.org/10.1038/s41598-020-](https://doi.org/10.1038/s41598-020-70413-3)
764 [70413-3](https://doi.org/10.1038/s41598-020-70413-3)
- 765 Moeini, M., Lu, X., Avti, P. K., Damseh, R., Bélanger, S., Picard, F., Boas, D., Kakkar, A., & Lesage, F. (2018).
766 Compromised microvascular oxygen delivery increases brain tissue vulnerability with age. *Scientific*
767 *Reports*, *8*(1). <https://doi.org/10.1038/s41598-018-26543-w>
- 768 Morland, C., Andersson, K. A., Haugen, Ø. P., Hadzic, A., Kleppa, L., Gille, A., Rinholm, J. E., Palibrk, V., Diget,
769 E. H., Kennedy, L. H., Stølen, T., Hennestad, E., Moldestad, O., Cai, Y., Puchades, M., Offermanns, S.,
770 Vervaeke, K., Bjørås, M., Wisløff, U., ... Bergersen, L. H. (2017). Exercise induces cerebral VEGF and
771 angiogenesis via the lactate receptor HCAR1. *Nature Communications*, *8*(1), 15557.
772 <https://doi.org/10.1038/ncomms15557>
- 773 Pantoni, L. (2010). Cerebral small vessel disease: from pathogenesis and clinical characteristics to therapeutic
774 challenges. In *The Lancet Neurology* (Vol. 9, Issue 7, pp. 689–701). [https://doi.org/10.1016/S1474-](https://doi.org/10.1016/S1474-4422(10)70104-6)
775 [4422\(10\)70104-6](https://doi.org/10.1016/S1474-4422(10)70104-6)
- 776 Radanovic, M., Pereira, F. R. S., Stella, F., Aprahamian, I., Ferreira, L. K., Forlenza, O. V., & Busatto, G. F. (2013).
777 White matter abnormalities associated with Alzheimer's disease and mild cognitive impairment: A critical
778 review of MRI studies. In *Expert Review of Neurotherapeutics* (Vol. 13, Issue 5, pp. 483–493).
779 <https://doi.org/10.1586/ern.13.45>
- 780 Reber, J., Hwang, K., Bowren, M., Bruss, J., Mukherjee, P., Tranel, D., & Boes, A. D. (2021). Cognitive
781 impairment after focal brain lesions is better predicted by damage to structural than functional network hubs.

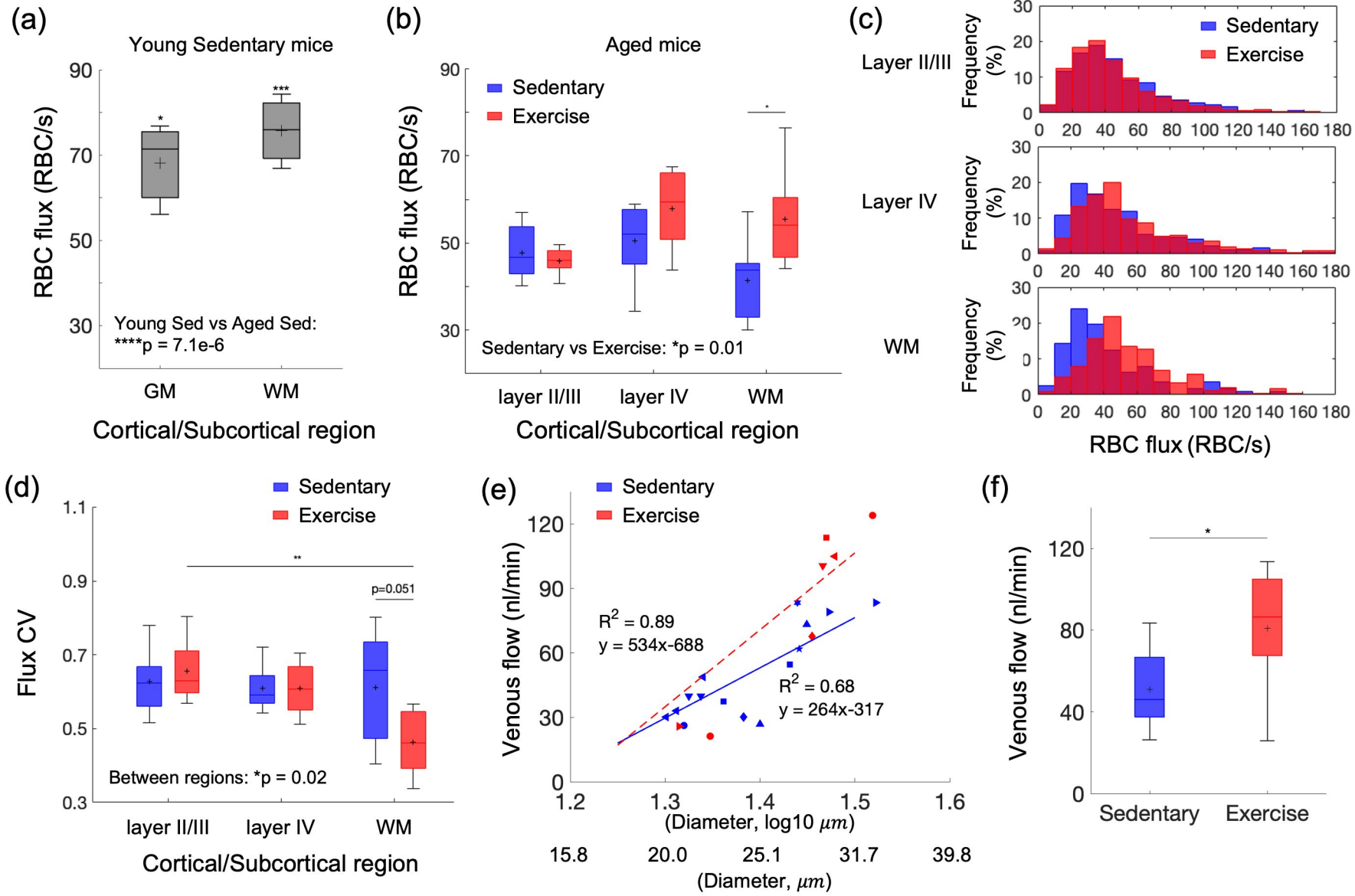
- 782 *Proceedings of the National Academy of Sciences*, 118(19). <https://doi.org/10.1073/pnas.2018784118/>-
783 /DCSupplemental
- 784 Sakadžić, S., Roussakis, E., Yaseen, M. A., Mandeville, E. T., Srinivasan, V. J., Arai, K., Ruvinskaya, S., Devor,
785 A., Lo, E. H., Vinogradov, S. A., & Boas, D. A. (2010). Two-photon high-resolution measurement of partial
786 pressure of oxygen in cerebral vasculature and tissue. *Nature Methods*, 7(9), 755–759.
787 <https://doi.org/10.1038/nmeth.1490>
- 788 Santisakultarm, T. P., Cornelius, N. R., Nishimura, N., Schafer, A. I., Silver, R. T., Doerschuk, P. C., Olbricht, W.
789 L., & Schaffer, C. B. (2012). In vivo two-photon excited fluorescence microscopy reveals cardiac- and
790 respiration-dependent pulsatile blood flow in cortical blood vessels in mice. *American Journal of*
791 *Physiology-Heart and Circulatory Physiology*, 302(7), H1367–H1377.
792 <https://doi.org/10.1152/ajpheart.00417.2011>
- 793 Seker, F. B., Fan, Z., Gesierich, B., Gaubert, M., Siemel, R. I., & Plesnila, N. (2021). Neurovascular Reactivity in
794 the Aging Mouse Brain Assessed by Laser Speckle Contrast Imaging and 2-Photon Microscopy:
795 Quantification by an Investigator-Independent Analysis Tool. *Frontiers in Neurology*, 12.
796 <https://doi.org/10.3389/fneur.2021.745770>
- 797 Şencan, İ., Espipova, T., Kılıç, K., Li, B., Desjardins, M., Yaseen, M. A., Wang, H., Porter, J. E., Kura, S., Fu, B.,
798 Secomb, T. W., Boas, D. A., Vinogradov, S. A., Devor, A., & Sakadžić, S. (2022). Optical measurement of
799 microvascular oxygenation and blood flow responses in awake mouse cortex during functional activation.
800 *Journal of Cerebral Blood Flow and Metabolism*, 42(3), 510–525.
801 <https://doi.org/10.1177/0271678X20928011>
- 802 Smith, E. E., & Markus, H. S. (2020). New Treatment Approaches to Modify the Course of Cerebral Small Vessel
803 Diseases. *Stroke*, 51(1), 38–46. <https://doi.org/10.1161/STROKEAHA.119.024150>
- 804 Snowdon, D. A., Greiner, L. H., Mortimer, J. A., Riley, K. P., Greiner, P. A., Markesbery, W. R., & Reprints, C.
805 (2011). Brain Infarction and the Clinical Expression of Alzheimer Disease The Nun Study From the
806 Sanders-Brown Center on Aging (Drs. *JAMA*.
- 807 Srinivasan, V. J., Atochin, D. N., Radhakrishnan, H., Jiang, J. Y., Ruvinskaya, S., Wu, W., Barry, S., Cable, A. E.,
808 Ayata, C., Huang, P. L., & Boas, D. A. (2011). Optical coherence tomography for the quantitative study of

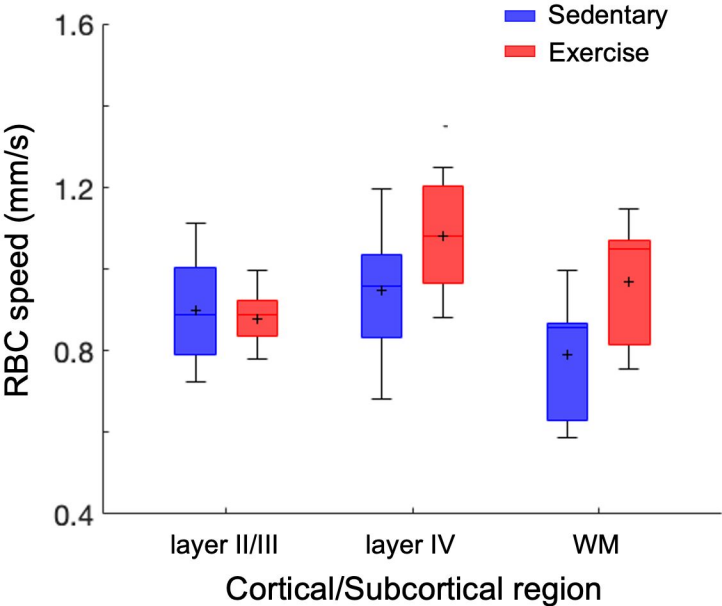
- 809 cerebrovascular physiology. *Journal of Cerebral Blood Flow and Metabolism*, 31(6), 1339–1345.
810 <https://doi.org/10.1038/jcbfm.2011.19>
- 811 Steventon, J. J., Chandler, H. L., Foster, C., Dingsdale, H., Germuska, M., Massey, T., Parker, G., Wise, R. G., &
812 Murphy, K. (2021). Changes in white matter microstructure and MRI-derived cerebral blood flow after 1-
813 week of exercise training. *Scientific Reports*, 11(1). <https://doi.org/10.1038/s41598-021-01630-7>
- 814 Tian, P., Devor, A., Sakadžić, S., Dale, A. M., & Boas, D. A. (2011). Monte Carlo simulation of the spatial
815 resolution and depth sensitivity of two-dimensional optical imaging of the brain. *Journal of Biomedical*
816 *Optics*, 16(1), 016006. <https://doi.org/10.1117/1.3533263>
- 817 Traschütz, A., Kummer, M. P., Schwartz, S., & Heneka, M. T. (2018). Variability and temporal dynamics of novel
818 object recognition in aging male C57BL/6 mice. *Behavioural Processes*, 157, 711–716.
819 <https://doi.org/10.1016/j.beproc.2017.11.009>
- 820 Tsai, P. S., Kaufhold, J. P., Blinder, P., Friedman, B., Drew, P. J., Karten, H. J., Lyden, P. D., & Kleinfeld, D.
821 (2009). Correlations of Neuronal and Microvascular Densities in Murine Cortex Revealed by Direct
822 Counting and Colocalization of Nuclei and Vessels. *Journal of Neuroscience*, 29(46), 14553–14570.
823 <https://doi.org/10.1523/JNEUROSCI.3287-09.2009>
- 824 Valenzuela, P. L., Castillo-García, A., Morales, J. S., de la Villa, P., Hampel, H., Emanuele, E., Lista, S., & Lucia,
825 A. (2020). Exercise benefits on Alzheimer’s disease: State-of-the-science. In *Ageing Research Reviews* (Vol.
826 62). Elsevier Ireland Ltd. <https://doi.org/10.1016/j.arr.2020.101108>
- 827 van Swieten, J. C., Geyskes, G. G., Derix, M. M. A., Peeck, B. M., Ramos, L. M. P., van Latum, J. C., & van Gijn,
828 J. (1991). Hypertension in the elderly is associated with white matter lesions and cognitive decline. *Annals*
829 *of Neurology*, 30(6), 825–830. <https://doi.org/10.1002/ana.410300612>
- 830 Wang, R., & Holsinger, R. M. D. (2018). Exercise-induced brain-derived neurotrophic factor expression:
831 Therapeutic implications for Alzheimer’s dementia. In *Ageing Research Reviews* (Vol. 48, pp. 109–121).
832 Elsevier Ireland Ltd. <https://doi.org/10.1016/j.arr.2018.10.002>
- 833 Winters, B. D. (2004). Double Dissociation between the Effects of Peri-Postrhinal Cortex and Hippocampal
834 Lesions on Tests of Object Recognition and Spatial Memory: Heterogeneity of Function within the Temporal
835 Lobe. *Journal of Neuroscience*, 24(26), 5901–5908. <https://doi.org/10.1523/JNEUROSCI.1346-04.2004>

- 836 Xiong, B., Li, A., Lou, Y., Chen, S., Long, B., Peng, J., Yang, Z., Xu, T., Yang, X., Li, X., Jiang, T., Luo, Q., &
837 Gong, H. (2017). Precise Cerebral Vascular Atlas in Stereotaxic Coordinates of Whole Mouse Brain.
838 *Frontiers in Neuroanatomy*, 11. <https://doi.org/10.3389/fnana.2017.00128>
- 839 Yaffe, K., Barnes, D., Nevitt, M., Lui, L.-Y., & Covinsky, K. (2001). A Prospective Study of Physical Activity and
840 Cognitive Decline in Elderly Women. *JAMA Internal Medicine*, 161(14), 1703–1708.
841 <https://jamanetwork.com/>
- 842
- 843
- 844
- 845









RBC line density (%)

Sedentary
Exercise

80
70
60
50
40
30

layer II/III

layer IV

WM

Cortical/Subcortical region

